International Tables for Crystallography (2018). Vol. H, Chapter 2.1, pp. 26–50.

2.1. Instrumentation for laboratory X-ray scattering techniques

A. Kern

2.1.1. Introduction

X-ray scattering techniques are among the most essential means of characterizing materials, as they are the most direct analytical methods for providing structural information for a material. In particular, X-ray powder diffraction has become one of the most important techniques in materials science, since many materials are first formed or are only available or used as powders or other polycrystalline forms.

The ever-increasing need for materials characterization, from basic research to industrial quality control, has led to a multitude of evolutionary and revolutionary instrument and application developments. In the past two decades, the capabilities and thus the range of application of laboratory X-ray diffractometers have increased exponentially.

The present chapter covers the full range of commonly used instrumentation for home-laboratory X-ray scattering analyses as detailed in Section 2.1.2, with the focus on powder diffraction. The scope is limited to recent and commercial designs, available off-the-shelf from the major manufacturers. Neither technologically obsolete nor niche instrumentation will be discussed. A short description of the history of X-ray instrumentation is given in Section 2.1.3, illustrating the significant technological advances made since 1985. Sections 2.1.4 to 2.1.7 describe the components of the diverse range of currently available home-laboratory X-ray powder diffractometers. The most important concepts are discussed here; for technological details the reader is referred to the original literature or to textbooks.

In order to maintain neutrality as well as timeliness, the use of brand names and photos of real equipment has been avoided.

2.1.2. Scope and terminology

An X-ray (powder) diffractometer is by definition an instrument for measuring X-ray diffraction phenomena (from powders), where 'diffraction' is defined as elastic, coherent scattering of X-rays from a crystal lattice (in the crystallographic literature, the terms 'diffraction', 'X-ray diffraction' and 'Bragg diffraction' are frequently used synonymously). In recent texts, a 'powder' is frequently defined as a 'solid containing small crystallites or particles that will flow when agitated' in accordance to the usual sense of the word in colloquial speech.

Such definitions for 'X-ray diffractometer' and 'powder' are problematic, as their scope is too narrow and arbitrarily limited. They are probably the result of the historical development of the methodology and the lack of interaction between groups representing different application areas, such as X-ray scattering, emission or absorption techniques. The application range and thus capabilities of today's instrumentation are neither comprehensively nor even appropriately described by their implicit limitation to measuring X-ray diffraction phenomena of crystalline solids in powdered form.

It is well known that scattering and thus interference phenomena will occur with any type of waves and obstacles, and are by no means restricted to X-rays or perfectly regular arrays of atoms exhibiting long-range order (X-ray diffraction). In general, X-ray scattering can provide information on the arrangement of atoms or particles in materials with short-range order or no order at all, like gases, liquids and amorphous solids. For this reason it is obvious that X-ray diffractometers are intrinsically suited (and are actually used) for a wide range of X-ray techniques beyond X-ray diffraction as defined above. These techniques not only comprise X-ray scattering from any solids or liquids with any degree of order, but also X-ray absorption (radiography) or X-ray emission (XRF) techniques, see also Section 2.1.4.3. Consequently, the following terminology will be used throughout the remainder of this chapter:

A *sample* is the object or quantity of material to be investigated, while the *specimen* is the representative portion of the sample that is actually prepared and analysed. Specimen properties such as microstructure and packing density may differ from the properties of the sample as a result of specimen preparation. This must be taken into account for selection of the appropriate instrument configuration, data acquisition and evaluation.

A *powder* is defined in EN-1330-11 (2007) as a 'large number of crystallites and/or particles (*i.e.* grains, agglomerates or aggregates; crystalline or non-crystalline) irrespective of any adhesion between them' and thus can be a loose powder (in the sense of common language), a solid block, a thin film or even a liquid. An *ideal powder* is represented by a virtually unlimited number of sufficiently sized, randomly oriented and spherical crystallites.

The term *X-ray diffractometer* will refer to an instrument that, in principle, is capable of doing any of the X-ray techniques mentioned above, further detailed in Section 2.1.4.3. Instrument components will be described independently of applications, as they are not exclusive to any application area. Note that the term X-ray diffractometer also explicitly includes 'film cameras'. This is worth mentioning, as even recent texts still differentiate between (i) cameras, originally characterized by the use of X-ray films, and (ii) diffractometers, originally defined as an instrument derived from a camera in which the film had been replaced by a point detector. In principle, any so-called cameras and any diffractometers can be equipped with any type of today's point, linear and area detectors, so the former distinction between cameras and diffractometers, which arose from the historical development of X-ray instrumentation, is completely obsolete.

2.1.3. Historical overview

2.1.3.1. *From film cameras to diffractometers*

2.1.3.1.1. *Film cameras*

Powder diffraction analysis started with the development of simple film cameras, right after von Laue formulated his basic diffraction theory and the Braggs, father and son, laid down the foundations of crystal structure analysis, in the years 1912–1914. The first and simplest cameras were developed independently by Debye & Scherrer (1916) and Hull (1917), using a film to detect the scattered X-rays, with the instrument geometry termed 'Debye–Scherrer geometry'. The basic drawback of Debye–Scherrer cameras was their lack of resolution. Consequently,

since standard X-ray tubes readily produce divergent beams, the next evolutionary step was to employ self-focusing geometries, as first proposed independently by Seemann (1919) and Bohlin (1920), termed 'Seemann–Bohlin geometry'. In addition to significantly improved resolution, the intensity was also greatly increased by using a para-focusing arrangement using an X-ray source and specimen with finite width (line focus). Guinier (1937) extended the Seemann–Bohlin geometry using an incident-beam monochromator. Although the monochromator significantly reduced the intensity, this disadvantage was overcompensated for by improved beam conditioning, leading to unparalleled resolution at that time and elimination of the $K\alpha_2$ component of the radiation. This made the Guinier camera the best-performing film camera at that time and it therefore enjoyed high popularity.

The idea of using powder diffraction for phase identification of substances in pure form or in mixtures, originally suggested by Hull (1919) and then formalized by Hanawalt *et al.* (1938), attracted enormous interest, and developed into the powder diffraction method, making it a fundamental tool for material scientists. However, while classic film cameras laid down the historical foundation for the success of polycrystalline diffraction, their use was mostly limited to phase identification, semi-quantitative phase analysis and macroscopic stress measurements. Inherent difficulties included, but were not limited to, obtaining reliable intensities (because of film grain size and nonlinearity of the film response), very limited flexibility in terms of hardware extensions such as non-ambient specimen stages, and lack of diffracted-beam conditioning (*e.g.* the use of diffracted-beam monochromators).

Detailed descriptions of the many camera types as well as their use are given in a large number of texts. The interested reader is specifically referred to the textbook of Klug & Alexander (1974), which also contains an extensive bibliography.

2.1.3.1.2. *Diffractometers*

Photographic films have two important weaknesses: the detection efficiency is low and quantification of the diffracted intensities, including the line-profile shapes, is indirect and cumbersome. These shortcomings led to the idea of replacing the film with a photon counter (most commonly utilizing the Geiger–Müller counter at that time) and thus to the development of a device called a 'diffractometer'. The design resembled that of the Bragg ionization spectrometer, but dispersed monochromatic radiation from lattice planes rather than a spectrum of X-ray wavelengths. The first diffractometer developed by Le Galley (1935) was a non-focusing arrangement using a point-focus X-ray tube, making use of the cylindrical geometry of a normal film camera. In subsequent instrument designs focusing geometries were adopted, mostly the 'Bragg–Brentano geometry' (Brentano, 1924), a modification of the Seemann–Bohlin geometry, first introduced by Lindemann & Trost (1940) and Friedmann (1945).

The introduction of the first commercial focusing diffractometer in the early 1950s resulted in another major advance of the polycrystalline diffraction method, and may be largely credited to Parrish and co-workers (*e.g.* Parrish, 1949). This instrument consisted of a fixed-anode X-ray tube and a mechanical goniometer, operating in Bragg–Brentano geometry. The initial replacement of photographic film by the Geiger–Müller counter, and soon after by scintillation and lithium-drifted silicon detectors, allowed accurate intensities and line-profile shapes with high resolution to be recorded. The large space around the specimen permitted the design of various interchangeable stages for specimen rotation and translation, automatic specimen changing and non-ambient analyses. As a consequence, powder diffraction found many new applications beyond phase identification, including, but not limited to, quantitative analysis of crystalline and amorphous phases, microstructure analysis, and texture and strain analysis, at ambient and non-ambient conditions.

In the following decades, diffractometers were fully automated, fully digitized, and electronically and mechanically stabilized. The data quality they delivered became generally superior to that of film cameras, including in terms of resolution, eventually even facilitating structure determination and refinement from powders. Attempts to improve Guinier or Seemann–Bohlin cameras by replacing the film with image plates or any other stationary or scanning detectors did not produce competitive instrumentation in terms of instrument flexibility and mechanical simplicity. As a result, film cameras were steadily replaced by automated diffractometers using the Bragg–Brentano geometry. Since the 1990s, classic film cameras as well as other Guinier- or Seemann–Bohlin-based instruments are no longer used in practical polycrystalline diffraction analysis and thus lost any commercial relevance, apart from for a few niche applications. The Bragg–Brentano geometry, as developed in the 1940s, became the dominating instrument geometry and accounted for more than 90% of all instruments sold. The remainder almost exclusively used Debye–Scherrer-type arrangements, either employing focusing incident-beam monochromators for flat-plate or capillary transmission setups, or parallel-beam setups based on (pinhole) slits and/or Soller collimators and/or channel-cut monochromators for micro-diffraction, small-angle X-ray scattering and the characterization of thin films.

While powder diffractometers have changed little in their construction and geometry since the 1940s, considerable advances have made in X-ray detection and X-ray beam conditioning (X-ray optics).

Significant detector developments include one- and two-dimensional position-sensitive detectors (PSDs) based on gas proportional counter technology, and especially that of the scanning one-dimensional PSD (Göbel, 1980). The replacement of a point detector by a scanning one-dimensional PSD allowed the measurement time required to record a full pattern to be reduced down to minutes without significant compromise on resolution. This enabled time-critical applications (such as non-ambient and high-throughput analyses), or compensation of the intensity loss when employing incident-beam monochromators.

The introduction of laterally graded multilayers on figured reflectors, so-called 'Göbel mirrors' (Schuster & Göbel, 1996), allowed the conversion of a convergent beam into a parallel beam, and thus added a new dimension to laboratory beam conditioning – at a time when X-ray techniques were expanding into the now very rapidly growing area of thin-film characterization, sparking a renaissance of the Debye–Scherrer geometry.

Until the late 1980s and early 1990s, traditional powder diffraction and thin-film characterization were seen as two different techniques with diverse requirements. As a consequence, thin-film techniques formed a different X-ray diffraction application sector, served by different and specialized instrumentation, in addition to the already existing distinction between single-crystal and powder diffraction applications and instrumentation. The X-ray powder diffraction market was characterized by dedicated (and separately marketed) instruments for traditional powder diffraction, usually based on the Bragg–

Brentano geometry, and for thin-film analysis, usually based on the Debye–Scherrer geometry.

2.1.3.2. *Recent years*

In the 1990s, more and more laboratories started to deal with a full range of materials and related applications - from powders through polycrystalline thin films to epitaxial thin films. Dedicated and inflexible instruments were no longer economic for serving the increasing range of applications and also their increasing data-quality requirements.

The growing need for multipurpose instrumentation led to a new generation of X-ray diffractometers in the late 1990s, from all of the major manufacturers, based on a platform concept covering all relevant beam-path components including X-ray sources, optics, specimen stages and detectors. This concept, described in Section 2.1.4, allowed for a faster development of more and more differentiated instrumentation to optimally meet the requirements of all possible applications and sample types. Particularly successful were design improvements that allow the user to transform an instrument on-site by changing beam-path components, often without any need for alignment or even tools, to cover a larger range of applications and sample types using a single instrument.

A major contribution to the platform concept came from the continued development of beam conditioners based on multilayers, resulting in a wealth of X-ray beam optics for different applications. Advanced sputtering techniques allow the fabrication of multilayer optics with virtually arbitrary beam divergence, which can be used to generate focusing, parallel and divergent beams for both point- and line-focus applications.

The introduction of a series of new detector technologies in the early 2000s represented another technological quantum leap, which completely changed the X-ray detection landscape for laboratory diffraction. Within only a few years, detectors based on silicon micro-strip, silicon pixel and micro-gap technologies reached a market share of more than 90% in newly sold systems. Proportional and scintillation point detectors will probably become obsolete in only a few years from now, but can still be found, usually in lower-budget systems.

Today's instruments, with their different possible configurations of beam-path components, are now capable of performing a wider range of X-ray scattering applications than ever (see Section 2.1.4.3). Not surprisingly, the platform concept has become so successful that all modern X-ray diffractometers are now, at least to some extent, equipped with interchange capabilities for beam-path components. However, the fundamental principles remain the same and date back to the first film cameras and diffractometers, no matter how advanced today's instrumentation is.

2.1.4. The platform concept – fitting the instrument to the need

Modern X-ray diffractometers are highly modular assembly systems based on a platform concept, with a shared set of major components over a number of distinct diffractometer models, serving different X-ray scattering application areas. Such a platform concept has two important advantages. Firstly, a common design allows differentiated instruments to be developed faster, and eases the integration of new or improved beam-path components, potentially over the whole model range. Secondly, it enables the design of an X-ray optical bench with on-site interchange capabilities, allowing the mounting of selected beam-path components to meet specific application and specimen-property requirements.

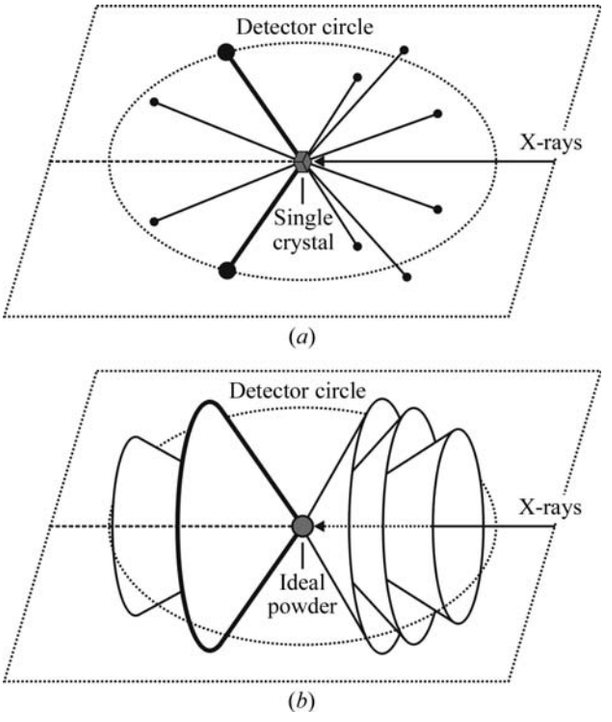

Figure 2.1.1
Diffraction of X-rays by (*a*) a rotating single crystal and (*b*) an ideal powder. The scattered intensity may be measured by a detector placed on the detector circle.

2.1.4.1. *Basic design principles and instrument geometry considerations*

X-ray scattering data are generally recorded in what is virtually the simplest possible manner, where the scattered intensity is measured by a detector mounted at some distance from the specimen. This is illustrated in Fig. 2.1.1, where a narrow, essentially monochromatic beam illuminates a small spherical specimen. For a rotating single crystal, the diffracted beams point in discrete directions in space as given by Bragg's law for each lattice vector d_{hkl} (Fig. 2.1.1*a*). For an ideal powder consisting of a virtually unlimited number of randomly oriented crystallites, the diffracted beams will form concentric cones ('Debye cones') with a semi-apex angle of 2θ, representing all randomly oriented identical lattice vectors d_{hkl} (Fig. 2.1.1*b*). Note that in contrast to a single crystal, an ideal powder does not need to be rotated to obtain a complete powder diffraction pattern.

Most instruments are built around a central specimen and consist of the following beam-path components, the numbering of which is consistent with the mounting positions shown in Fig. 2.1.2:

(1) X-ray source;
(2) incident-beam optics;
(3) goniometer base or specimen stage;
(4) diffracted-beam optics;
(5) detector.

The directions of the *incident* and *diffracted beams* (also called 'primary' and 'secondary' beams) form the *diffraction plane* (also called the 'equatorial plane' or 'scattering plane'). The goniometer base can be mounted horizontally (horizontal diffraction plane) or vertically (vertical diffraction plane). The direction perpendicular to the equatorial plane is known as the *axial*

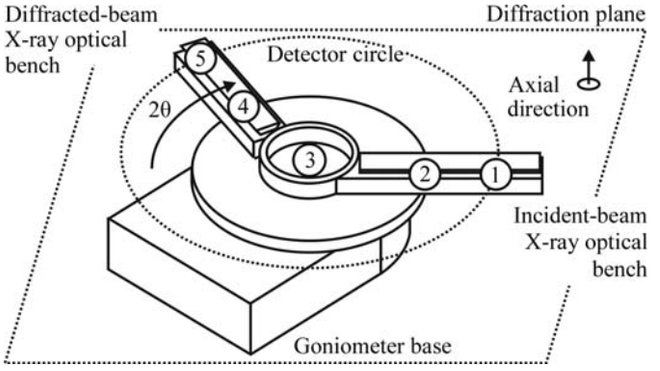

Figure 2.1.2
The basic design principle of modern diffractometers. Currently available instruments are built around a centrally mounted specimen and represent an X-ray optical bench with mounting positions for any (1) X-ray sources, (2) incident-beam optics, (3) specimen stages, (4) diffracted-beam optics and (5) detectors. The 2θ position of the scattered-X-ray optical bench refers to the 2θ angle of the Debye cone shown in bold in Fig. 2.1.1(*b*).

direction. The *detector circle* (also called the 'goniometer circle' or 'diffractometer circle') is defined either by the centre of the active window of a stationary detector, or, in most cases, by a detector moving around the specimen, and is coplanar to the diffraction plane. The 2θ angle of both the diffracted beam in Fig. 2.1.1(*a*) and the Debye cone in Fig. 2.1.1(*b*) (shown in bold) refers to the 2θ position of the diffracted-beam X-ray optical bench in Fig. 2.1.2. It is obvious from Figs. 2.1.1 and 2.1.2 that, in principle, diffraction from single crystals and (ideal) powders can be measured using the same instrument.

An instrument design with a centrally mounted specimen has the important advantage that it implicitly allows the operation of one and the same instrument in both Bragg–Brentano and Debye–Scherrer geometry, depending on the beam divergence chosen. The actual instrument geometry is thus a function of the actual beam propagation angle (divergent, parallel or convergent), making the X-ray optics the most important part of any instrument-geometry conversion. The relationship between the two geometries and their implementation in a single instrument using an incident-beam X-ray optical bench is illustrated in Fig. 2.1.3.

As laboratory X-ray sources invariably produce divergent beams, the 'natural' instrument geometry is self-focusing, 'automatically' leading to the Bragg–Brentano geometry as shown in Fig. 2.1.3(*a*). In this geometry the angle of both the incident and the diffracted beam is θ with respect to the specimen surface. The X-ray-source-to-specimen and the specimen-to-detector distances are equal. The diffraction pattern is collected by varying the incidence angle of the incident beam by θ and the diffracted-beam angle by 2θ. The focusing circle is defined as positioned tangentially to the specimen surface. The focusing condition is fulfilled at the points where the goniometer circle intersects the focusing circle, and thus requires measurements in reflection mode.

The Bragg–Brentano geometry may be extended by an incident- or a diffracted-beam monochromator. In the case of an incident-beam monochromator as shown in Fig. 2.1.3(*b*), the focus of the X-ray source is replaced by the focus of the monochromator crystal. This involves mounting the monochromator crystal (and the X-ray source) a certain distance away along the incident-beam X-ray optical bench, as given by the focusing length of the monochromator crystal (the dotted line in Fig. 2.1.3*b*). For a diffracted-beam monochromator or mirror, the geometry shown in Fig. 2.1.3(*b*) can be thought of as reversed (simply consider the X-ray source and detector switching their positions).

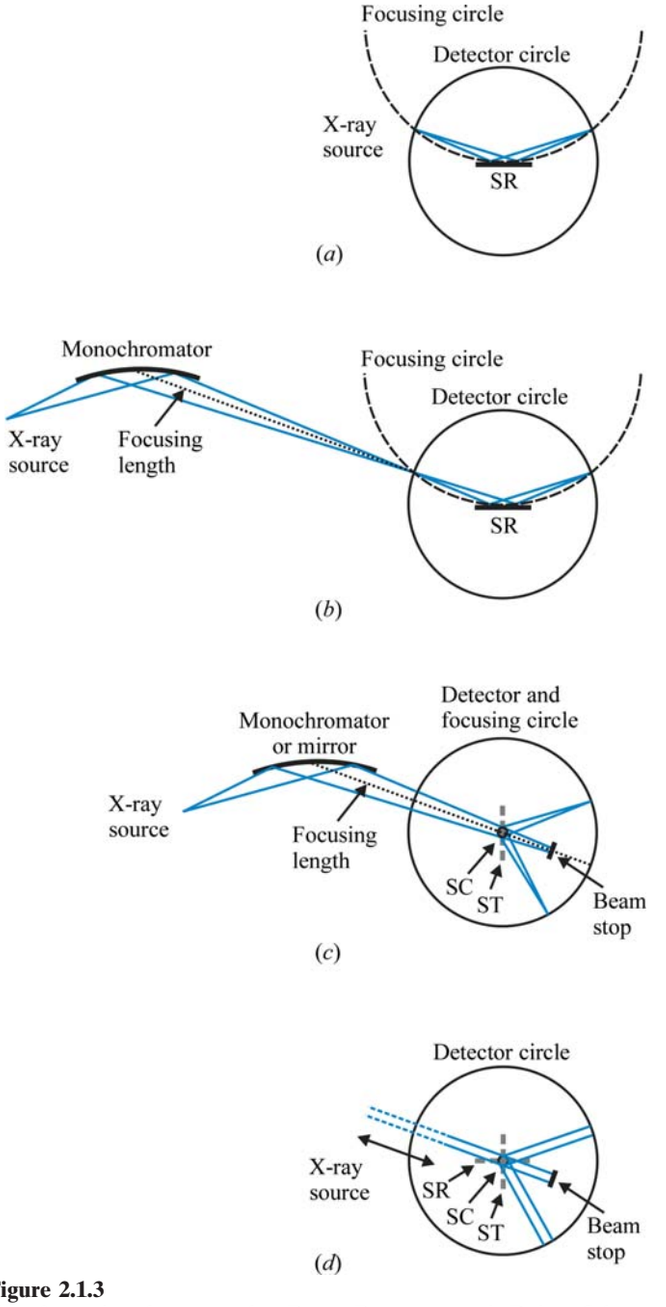

Figure 2.1.3
Transformation between the Bragg–Brentano and Debye–Scherrer geometries using a incident-beam X-ray optical bench. SR: flat specimen, reflection mode; SC: capillary specimen, transmission mode; ST: flat specimen, transmission mode. The actual instrument geometry is a function of the actual beam-propagation angle, making the X-ray optics the most important part of any instrument-geometry conversion. (*a*) Divergent beam: Bragg–Brentano geometry, (*b*) divergent beam: Bragg–Brentano geometry extended by an incident-beam monochromator. (*c*) Convergent beam: focusing Debye–Scherrer geometry, (*d*) parallel beam: Debye–Scherrer geometry. Transformation is achieved by mounting the X-ray tube and pre-aligned optical components at predefined positions of the optical bench. None of the figures are to scale.

The conversion from Bragg–Brentano to Debye–Scherrer geometry involves the mounting of some kind of optics designed to convert the divergent beam coming from the X-ray source into a focusing or parallel beam; this is shown in Figs. 2.1.3(*c*) and (*d*), respectively.

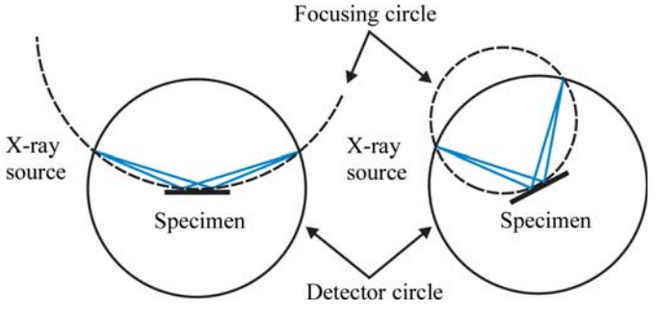

Figure 2.1.4
Bragg–Brentano geometry. The focusing circle, given for two different angles 2θ, is tangential to the specimen surface. Its diameter is given by the intersections between the detector and the focusing circles and is thus 2θ dependent.

In a focusing Debye–Scherrer geometry setup, as shown in Fig. 2.1.3(*c*), the divergent beam coming from the X-ray source is normally focused on the detector circle (for highest resolution) by means of an incident-beam monochromator or a focusing mirror. The focusing circle is identical to the detector circle and the focusing condition requires measurements in transmission mode. When employing an incident-beam monochromator with sufficient focusing length, then conversion between the Bragg–Brentano geometry and the focusing Debye–Scherrer geometry involves a shift of the monochromator crystal (and the X-ray source) along the incident-beam X-ray optical bench (note the identical focusing length of the monochromator shown in Figs. 2.1.3*b* and *c*).

For a parallel-beam setup, as shown in Fig. 2.1.3(*d*), parallelization of the divergent beam coming from the X-ray source may be achieved by different means, such as collimators (classic Debye–Scherrer geometry) or reflective optics such as mirrors or capillaries. In principle, the X-ray source and the detector may be placed at any distance from the specimen, as there are no focusing requirements. As a consequence, measurements can be performed in both reflection and transmission mode.

In a simplified scheme, conversion between the geometries discussed above involves repositioning of the X-ray source, together with mounting of X-ray optics with suitable beam divergence. To make this possible, the incident-beam optical X-ray bench offers the necessary predefined mounting positions including relevant translationary and rotationary degrees of freedom.

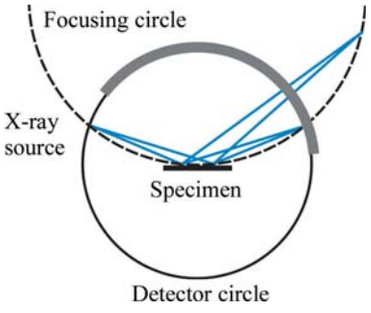

Figure 2.1.5
Bragg–Brentano geometry. While all diffracted beams focus on the (variable-diameter) focusing circle (here shown for two beams), focusing on the detector circle is only achieved at the X-ray source and detector positions (located at the intersections between the detector and the focusing circles). This prevents the use of larger position-sensitive detectors because of defocusing, as indicated by the hypothetical large position-sensitive detector represented by the bold grey line.

An important aspect directly related to the choice of the instrument geometry is the geometric compatibility with position-sensitive detectors. In contrast to Debye–Scherrer geometry, large line and area detectors may not be used in Bragg–Brentano geometry. This is an important limitation of the latter, as the focusing circle does not coincide with the detector circle and has a 2θ-dependent diameter, as illustrated in Fig. 2.1.4. As a consequence, the diffracted beam is only focused on a single point of the goniometer circle, as shown in Fig. 2.1.5. However, small position-sensitive detectors with an angular coverage of not more than about 10° 2θ are used with great success, as defocusing can be ignored at diffraction angles larger than about 20° 2θ if high angular accuracy and resolution are not required. For measurements at smaller 2θ angles, or for highest angular accuracy and resolution, the active window size of a position-sensitive detector may be reduced by means of slits and/or electronically down to a point, allowing the use of this detector as a point detector.

2.1.4.2. *Range of hardware*

An X-ray diffractometer is generally characterized by the relationship between a conditioned beam, the specimen orientation and the subsequent interception of the diffracted beams by a detector of given geometry and imaging properties. There are only a very few instrument configurations that will be ideal for any two application areas, or every conceivable sample within a single application area. It is the user's responsibility to match the instrument to the specimen properties, which can be challenging, particularly in multi-user environments with a large variety of sample types. The platform and the X-ray optical-bench concepts allow the user to choose and mount the most appropriate beam-path components in order to optimize an instrument with respect to a specific application and specimen-property requirements. Table 2.1.1 provides an overview of the currently available types of beam-path components from the X-ray source through to the detector.

The length of available X-ray optical benches varies, and is typically in the range of about 15 cm up to 100 cm. Larger benches allow mounting of bulky components (*e.g.* moving-target X-ray sources or large detectors) as well as mounting of several X-ray optics in a row (*e.g.* combinations of mirrors and channel-cut monochromators). Some diffractometer models allow mounting of two incident- and/or diffracted-beam X-ray optical benches to mount different beam-path components in parallel, *e.g.* X-ray sources with different wavelengths or beam shapes (very popular in single-crystal diffraction), X-ray optics with different beam divergence (*e.g.* to switch between Bragg–Brentano and Debye–Scherrer geometry), and different detector types.

While Table 2.1.1 and the above may imply an enormous combinatorial diversity, in practice this is not entirely the case. In general, beam-path components have to be compatible with the selected instrument geometry, which is dictated by the choice of the X-ray source (point or line), the beam characteristics (wavelength distribution, divergence) and the detector (point, linear or area). This automatically narrows down the range of combinations. As an obvious example, many crystal monochromators and X-ray mirrors are only compatible with a particular wavelength. Also, the size and weight of bulky components, such as moving-target X-ray sources, large specimen stages and large two-dimensional detectors, may impose practical constraints that require consideration. For example, the acces-

Table 2.1.1
Types of beam-path components available in laboratory X-ray powder diffraction

The column numbering corresponds to the positions indicated in Fig. 2.1.2 at which individual components can be mounted.

Position 1	Positions 2 and 4	Position 3		Position 5
X-ray sources	X-ray optics	Goniometer base	Specimen stages	Detectors
Fixed target Moving target (rotating anodes, liquid-metal jets)	Absorptive (apertures, metal filters) Diffractive (monochromators, analysers) Reflective (multilayer mirrors, capillary optics)	Vertical [ω–θ (θ–θ), ω–2θ (θ–2θ)] Horizontal [ω–θ (θ–θ), ω–2θ (θ–2θ)]	Fixed, rotating Specimen changer Eulerian cradles Kappa stages Tilt/fixed χ stages *XYZ* stages Flow-through cells Non-ambient (low temperature, high temperature, humidity, high pressure)	Scintillation Gas ionization (metal wire, micro-gap) Semiconductor (SiLi, strip/pixel, CCD/CMOS)

sible angular range may be limited for large components owing to collision issues, while heavy loads on vertical goniometers may impede alignment and lead to early wear and tear. Restrictions will be discussed in Sections 2.1.5 to 2.1.7 for the individual components.

These days, the exchange of lighter components, such as most X-ray optics, specimen stages and detectors, does not require any tools at all (such as when a snap-lock mechanism is employed) or more than a few screws for fixing. Alignment is normally not required when components are factory pre-aligned and handled with care, and when mounts are manufactured with good quality. Intrinsic changes of the beam direction (*e.g.* focusing crystal monochromators or X-ray mirrors) or beam offsets (*e.g.* two-bounce channel-cut monochromators) need compensating translation and/or rotation of the components involved.

The exchange of large, heavy components, or complicated rebuildings such as the conversion of a goniometer (vertical $\leftrightarrow$ horizontal, θ–$\theta \leftrightarrow \theta$–2$\theta$ *etc.*), may be still possible for technically skilled users. However, special tools may be necessary, requiring shipment of the component(s), or even the instrument, back into the factory. In addition, X-ray, machine and electrical safety directives by the local authorities have to be obeyed, and conversions may require updating approval to use the instrument. In such cases it may be more economic to operate two dedicated instruments instead.

The instrument control software plays a particularly important role in the context of instrument configuration and automated instrument conversion. In modern instruments, each beam-path component is equipped with an identification chip or hole masks read out by light barriers, which uniquely identify the respective component and link it with all its individual stored or coded properties. This information may range from part numbers, usage history or alignment information such as beam offsets, through to a virtually unlimited wealth of any physical data required to configure and operate that particular component. This 'component recognition' feature provides for completely new and important capabilities of laboratory powder diffractometers, the most important of which are:

(*a*) Any beam-path components, and each change of status, can be automatically detected, validated and configured, allowing true 'plug & play' operation.

(*b*) Real-time conflict detection: detection of incompatible, incorrectly mounted or missing instrument components. This feature can also help the user in choosing compatible instrument components, as already discussed above.

(*c*) Automatic, motorized adjustments of beam direction or beam-offset changes, based on the information stored in the related components' ID chips, as individually determined at the factory *via* pre-alignment.

(*d*) Every instrument detail can be saved together with the measurement data, providing for a complete and accurate documentation of the experiment. In principle, every measurement can be exactly reproduced even years later.

(*e*) Measurement instructions can include instrument information. For example, manufacturers or users can configure the measurement software to propose instrument configurations deemed best for particular applications. A user with appropriate rights can choose to enforce a certain instrument configuration so that measurements will not start unless the instrument has detected the required configuration.

Both the platform concept and the huge advances in instrumentation and instrument control software have dramatically changed the laboratory X-ray instrumentation landscape in the past few years. The ease with which an instrument configuration can be changed is not only useful for less-skilled users. Probably even more importantly, it allows the use of the same instrument, in different configurations, for different X-ray application areas. It can generally be said that laboratory X-ray instrumentation has overcome the (mostly historical) dividing lines between different applications, which were mostly between single-crystal diffraction, powder diffraction and thin-film analysis. As far as differences still remain, these are usually solely the consequence of dedicated instrument components for meeting specific application requirements, resulting in specialized measurement and data-evaluation software, which is rarely included with each instrument.

2.1.4.3. *Range of applications*

It is the flexibility of today's X-ray diffractometers that leads to their usefulness for a wide range of X-ray scattering techniques beyond traditional X-ray powder 'Bragg diffraction'. Table 2.1.2 provides an overview.

X-ray scattering techniques represent the vast majority of techniques that X-ray diffractometers are used for. Properly configured, however, the same instrument can also be used to collect X-ray absorption (X-ray radiography) or X-ray emission (X-ray fluorescence) data, even if the achievable data quality cannot compete with dedicated instruments.

For X-ray radiography, an instrument will be configured in transmission geometry with the X-rays projected towards a

Table 2.1.2
X-ray applications for with modern X-ray diffractometers

X-ray scattering
Powder diffraction
Qualitative (phase identification) and quantitative phase analysis
Indexing, structure determination and structure refinement from powder data
Microstructure analysis (texture, size, strain, microstrain, disorder and other defects)
Pair distribution function analysis ('total scattering')
Thin-film analysis
Grazing incidence X-ray diffraction (GIXRD)
X-ray reflectometry
Stress and texture
High-resolution X-ray diffraction
Reciprocal-space mapping
In-plane GIXRD
Single-crystal diffraction
Chemical crystallography
Protein crystallography
Small-angle X-ray scattering
X-ray topography
X-ray absorption
X-ray radiography (X-ray-absorption-based imaging)
X-ray emission
X-ray fluorescence

specimen. X-rays that pass through the specimen can be detected to give a two-dimensional representation of the absorption contrast within the specimen. For tomography, the X-ray source and detector will be moved to blur out structures not in the focal plane. Multiple images can be used to generate a three-dimensional representation of the specimen by means of computed tomography. Obvious disadvantages are the large effective focal spot size of the X-ray sources and the relatively low resolution of the detectors that are typically used for powder diffraction, which, in combination with a limited adjustability of both the X-ray-source-to-specimen and specimen-to-detector distances, lead to substantial unsharpness issues and poor resolution. High-quality images can be achieved when using micro-focus X-ray sources and charge-coupled device (CCD) detectors with focus and pixel sizes smaller than 10 μm, respectively, but such an instrument configuration is not suitable for applications requiring ideal powders (see also Sections 2.1.6 and 2.1.7).

Collecting X-ray fluorescence data is comparatively straightforward. Data can be collected simultaneously to X-ray scattering data when employing a suitable detector, such as an energy-dispersive detector (Section 2.1.7.2.3). There are a couple of disadvantages to be considered, such as absorption issues (the specimen will be normally measured in air rather than in vacuum, hampering the analysis of light elements) and the inefficiency of excitation by the characteristic line energies of the X-ray source anode materials typically used for diffraction (hampering the analysis of elements with higher atomic numbers than that of the anode material).

2.1.5. Goniometer designs

A goniometer, by definition, is an instrument that either measures an angle or allows an object to be rotated to a precise angular position. In an X-ray diffractometer the purpose of the goniometer is to move the X-ray source, specimen and detector in relation to each other. Goniometers are usually categorized by the number of axes available for X-ray source, specimen and detector rotation, and are thus called one-, two-, three-, ..., n-axis (or -circle) goniometers.

Because of practical reasons, most goniometers consist of two distinct components, a goniometer base and a specimen stage, with the specimen stage mounted on the goniometer base.

The goniometer base typically offers two axes, one axis to rotate the X-ray source or the specimen stage, the other axis to rotate the detector. In some designs goniometer bases are omitted, specifically if there is no need to move the X-ray source and the detector, such as in Debye–Scherrer-type diffractometers with large detectors. Such machines are usually dedicated to a particular application without the need for high flexibility.

Depending on the requirements of the application, additional rotational and translational degrees of freedom may be needed to rotate and translate a specimen in space; these are usually implemented in the specimen stage. More rotational degrees of freedom may include the rotation of the X-ray source line focus or a rotation of the detector out of the diffraction plane to measure diffraction by lattice planes (nearly) perpendicular to the specimen surface, so-called non-coplanar diffraction.

2.1.5.1. *Geometrical conventions and scan modes*

In the literature there is some inconsistency related to the naming of axes and the choice of signs for angles (left- *versus* right-handed). A comprehensive treatment of geometrical conventions has recently been given by He (2009); in the following these conventions will be adhered to.

In many texts the notations θ–2θ and θ–θ rather than ω–2θ and ω–θ are used, mostly because of historical reasons. The first diffractometers operated in Bragg–Brentano geometry (see Section 2.1.3.1.2) and were equipped with single-axis goniometers. In such a goniometer the single axis drives two shafts which are mechanically coupled 1:2 or 1:1; thus the notations θ–2θ and θ–θ were coined. Today, the majority of all goniometer bases allow coupled as well as uncoupled rotation of the ω and θ axes. Therefore the ω–2θ and ω–θ notations should be generally preferred, as they represent the more general notations.

2.1.5.1.1. *Goniometer base*

A typical goniometer base provides two coaxial and independently driven axes, ω and 2θ, mounted perpendicular to the diffraction plane. These two axes are the main axes of a goniometer, since they have the most effect on the accuracy and precision of measured Bragg angles. The diffraction plane and the axes are generally described by a right-handed Cartesian coordinate system, as illustrated in Fig. 2.1.6, where the direct X-ray beam propagates along the X_L axis. Z_L is up and coincident with the ω and 2θ axes, and X_L–Y_L define the diffraction plane with the detector circle coplanar to it. Since X_L is coincident with the incident X-ray beam, it is also the axis of the Debye cones. The semi-apex angles of the cones are determined by the 2θ values given by the Bragg equation. The angles 2θ and γ describe the direction of scattering vectors in space (compare Fig. 2.1.1), where γ is defined as the azimuthal angle from the origin at $-Z_L$ with a right-hand rotation axis along the opposite direction of the incident beam ($-X_L$ direction).

The ω and 2θ axes are mechanically arranged as the inner circle and outer circle, respectively. The inner circle usually carries either the specimen stage or the X-ray source, while the detector is mounted on the outer circle. As a consequence, there are two common base goniometer configurations in use: In the ω–2θ (or θ–2θ with $\omega = \theta$) configuration, the incident-beam direction is

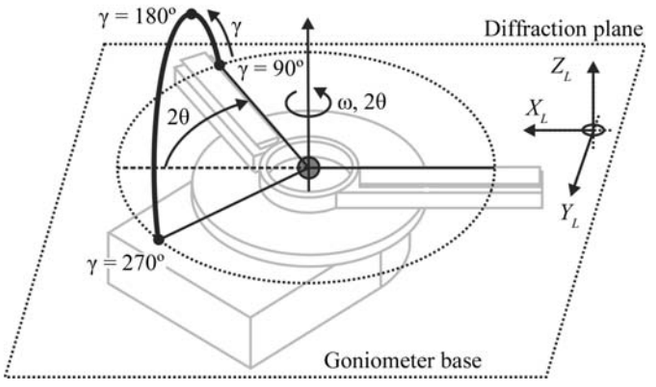

Figure 2.1.6
Laboratory coordinates and geometric definition of the coaxial goniometer axes ω and 2θ. If the azimuthal angle γ takes all values from 0 to 360° at a given Bragg angle 2θ, the trace of the diffracted beams forms a Debye cone (compare with Fig. 2.1.1).

mechanically fixed. The ω axis rotates the specimen stage, while the 2θ axis rotates the detector. In the ω–θ (or θ–θ with $\omega = \theta$) configuration, the ω axis defines the incident-beam angle by rotating the X-ray source, while the other axis scans the detector. In this configuration the specimen stage is mechanically fixed. Both configurations allow identical positioning of the X-ray source, specimen and detector relative to each other.

The goniometer base orientation is defined by the diffraction plane, which can be either horizontal or vertical. Vertical-base goniometers in ω–θ configuration are particularly popular, as the specimen is always kept horizontal, effectively preventing it from falling off. However, heavy specimens and beam-path components require particular attention in both the goniometer base design and choice of orientation, as they have a strong impact on goniometer accuracy, precision and early wear and tear (see also Section 2.1.5.2). Where loads exceed the maximum specifications for a vertically mounted goniometer base, and whenever horizontal specimen positioning is not imperative, either a vertical goniometer base in ω–2θ configuration or a horizontal goniometer should be chosen.

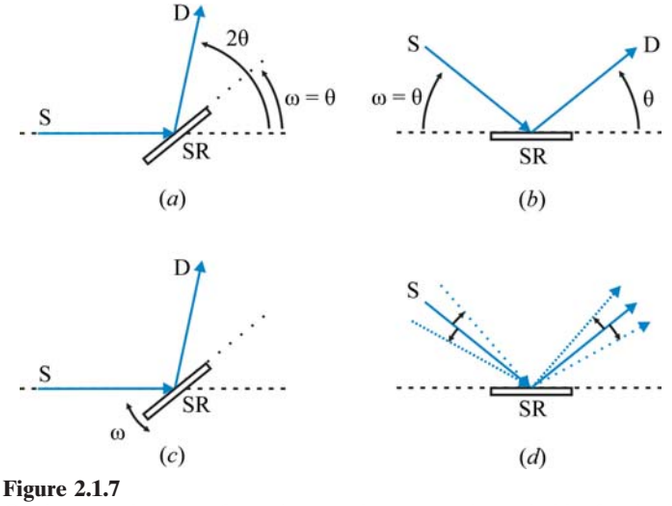

Figure 2.1.7
Goniometer base configurations and scan modes suitable for both Bragg–Brentano or Debye–Scherrer geometry. Symmetric beam path setup in (*a*) ω–2θ and (*b*) ω–θ configuration. Rocking curve setup in (*c*) ω–2θ and (*d*) ω–θ configuration. Only the central beams are shown for clarity, rotations are indicated by arrows. S: X-ray source, D: detector, SR: flat specimen, reflection mode.

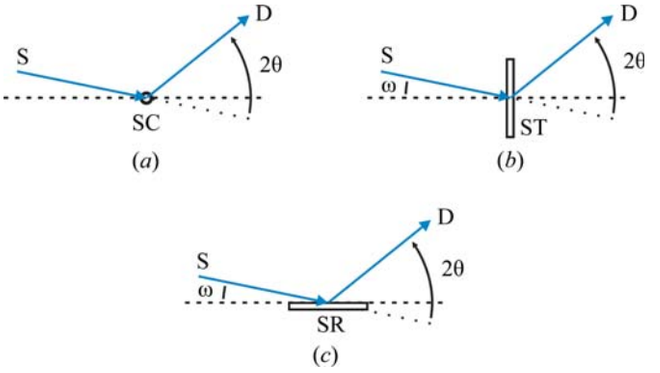

Figure 2.1.8
Goniometer base configurations and scan modes suitable for the Debye–Scherrer geometry only. Only the central beams are shown for clarity. (*a*) Capillary specimen in transmission mode, (*b*) flat specimen in transmission mode, (*c*) flat specimen in reflection mode, grazing incidence with fixed ω. S: X-ray source, D: detector, SR: flat specimen, reflection mode; SC: capillary specimen, transmission mode; ST: flat specimen, transmission mode.

In Figs. 2.1.7 and 2.1.8 a range of typical goniometer base configurations and scan modes are illustrated.

A symmetric beam-path setup in reflection mode, where both the incident and diffracted beam form an angle of θ with respect to the specimen surface, is mandatory for instruments operating in Bragg–Brentano geometry to maintain the focusing condition (see Section 2.1.4.1), but is also commonly used in Debye–Scherrer geometry. Scanning involves coupling of the ω (with $\omega = \theta$) and 2θ axes in a ratio of 1:2 for the ω–2θ configuration (Fig. 2.1.7*a*) and 1:1 for the ω–θ configuration (Fig. 2.1.7*b*), but only allows probing of lattice planes essentially parallel to the specimen surface. Where determination of a texture parameter is sought, a so-called 'rocking-curve' measurement can be performed by rocking either the specimen or the X-ray source and detector around the position of a Bragg peak. Two scenarios need to be considered and are illustrated in Fig. 2.1.7(*c*) and Fig. 2.1.7(*d*). In the ω–2θ configuration with fixed X-ray source (Fig. 2.1.7*c*), the detector will be fixed at the 2θ position of a selected Bragg peak, while the specimen is rotated ('rocked') independently, to perform a so-called 'ω-scan'. To achieve the same in an ω–θ configuration with fixed specimen, the X-ray source and the detector will be coupled 1:−1 or −1:1 to perform a clockwise or anticlockwise scan while maintaining the selected 2θ position, respectively, as illustrated in Fig. 2.1.7(*d*).

In Debye–Scherrer geometry there is no geometrical restraint requiring coupled scans to maintain 2θ-dependent focusing conditions, as is the case in the Bragg–Brentano geometry, providing high flexibility. Specimens can be measured in both reflection as well as transmission mode. In principle, the incident-beam direction may be any relative to the specimen surface, and can be fixed or variable, while the detector performs a 'detector scan'. The ω and 2θ axes may be coupled or not. Choices solely depend on the specimen properties and the requirements of the application. This is demonstrated in Fig. 2.1.8 for a few representative examples. The classic Debye–Scherrer geometry using a capillary specimen is shown in Fig. 2.1.8(*a*). The capillary specimen can be readily exchanged for a flat-plate specimen as shown in Fig. 2.1.8(*b*) and Fig. 2.1.8(*c*) for flat-plate transmission and reflection, respectively. ω can be set to different angles or perform a coupled scan to allow access to higher 2θ angles (Fig. 2.1.8*b*) or can be set to a different angle for grazing-incidence measurements (Fig. 2.1.8*c*). In some applications it may be beneficial to perform a (usually coupled) scan of both ω and 2θ to

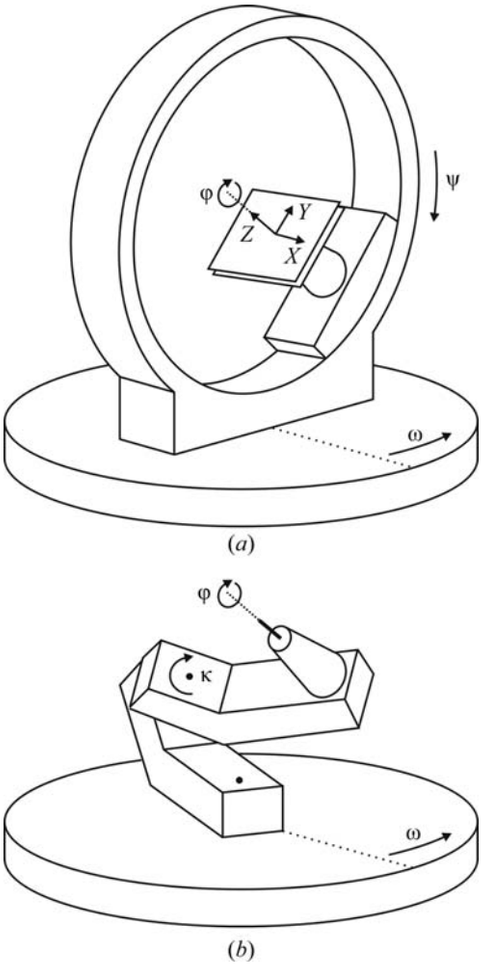

Figure 2.1.9
Geometric definition of the Eulerian and kappa geometries with identical specimen orientation in space. (*a*) Specimen rotation and translation in a Eulerian cradle equipped with an *XYZ* stage, (*b*) specimen rotation on a kappa stage.

improve particle statistics ('wobbling'). Obviously, all the setups shown in Fig. 2.1.8 will work for the full range of X-ray scattering and absorption techniques as discussed in Section 2.1.4.3, leading to the renaissance of the Debye–Scherrer geometry within the past 20 years.

2.1.5.1.2. *Specimen stage*

Depending on the requirements of the application, the specimen stage may offer additional degrees of freedom for specimen rotation as well as *X*, *Y*, *Z* translation. The goniometer base may be configured as ω–2θ as well as ω–θ, and may be oriented vertically as well as horizontally.

To orient a specimen in all possible orientations in space, the specimen stage will offer two more rotational degrees of freedom in addition to the ω and 2θ axes provided by the goniometer base. Such goniometers are known as four-axis diffractometers, with two basic geometries in common use for specimen orientation: Eulerian geometry and kappa geometry.

In the Eulerian geometry the specimen is oriented through the three Euler angles ω (defined by the ω axis of the goniometer base), ψ (psi), and φ (phi). The relationship between the laboratory and rotation axes is shown in Fig. 2.1.9(*a*) for a typical Eulerian cradle. The ω angle is defined as a right-handed rotation about the ω (or Z_L) axis. The ψ angle is a right-hand rotation about the ψ axis, which lies in the diffraction plane and runs parallel to the bisectrix between the incident and diffracted beams. The φ angle defines a left-handed rotation about an axis on the specimen, typically the normal to a flat specimen surface. In some texts the angle χ (chi) is used instead of ψ, with the relationship between the two angles defined as $\psi = 90 - \chi$. Eulerian cradles have the advantage of high mechanical stability and are often integrated with *XYZ* stages to handle bulky specimens. The geometrical definitions of specimen *X*, *Y*, *Z* translations are also shown in Fig. 2.1.9(*a*).

The kappa (κ) geometry shown in Fig. 2.1.9(*b*) represents an alternative way to orient a specimen in space. The ψ axis of the Eulerian geometry is replaced by the κ axis, which is tilted at 50° relative to the diffraction plane. It supports an arm carrying the specimen, with the φ axis tilted at 50° to κ. The role of the Eulerian ψ rotation is fulfilled by means of combined rotation along κ and φ, which allows Eulerian ψ angles in the range −100 to +100° to be obtained. The absence of the (bulky) ψ circle of Eulerian cradles allows an unobstructed view of the specimen and unhindered access from 'above', for example to mount a cooling device without risk of collision. These two advantages made the kappa geometry popular in single-crystal work. On the other hand, it is not possible to move the specimen to an 'upside-down' position, *i.e.* equivalent to Eulerian ψ angles less than −100° or greater than 100°.

Most goniometers do not offer all six rotational and translational degrees of freedom. The majority of these are actually three-axis goniometers, where the specimen stage offers one additional axis for specimen rotation.

A comprehensive overview of commercially available specimen stages is beyond the scope of this chapter owing to the huge number of dedicated specimen stages available for different kinds of specimen types, levels of automation and non-ambient analyses. The most complete and most current information will be found in manufacturers' product information.

2.1.5.2. *Accuracy and precision*

Particularly high demands are made on goniometer accuracy and precision in Bragg-angle positioning (goniometer base) and specimen orientation (specimen stage). These are usually expressed by the angular accuracy and precision of the goniometer-base axes (ω, 2θ) and the sphere of confusion of specimen positioning in space. A detailed discussion is given by He (2009).

Depending on the application and the actual instrument configuration, additional requirements may be imposed on goniometers, and may limit the maximum accuracy and precision that are achievable. Typical requirements, often not compatible with each other, are:

(*a*) mounting of heavy and bulky beam-path components and specimens;
(*b*) variable goniometer radii, typically ranging from about 15 to 60 cm; and
(*c*) vertical goniometer operation to prevent specimens from falling off the holder.

Each of these requirements may have an impact on goniometer accuracy and precision, and potential early wear and tear. Typical loads range from several kg for fixed-target X-ray sources up to 50 kg and more for moving-target X-ray sources. Small detectors such as point and one-dimensional detectors range from less than 1 kg up to a few kg, while large two-dimensional detectors may weigh up to 50 kg and sometimes even more.

For vertical goniometers, the loads on the main axis bearings can be effectively reduced by counterbalances, as shown in Fig.

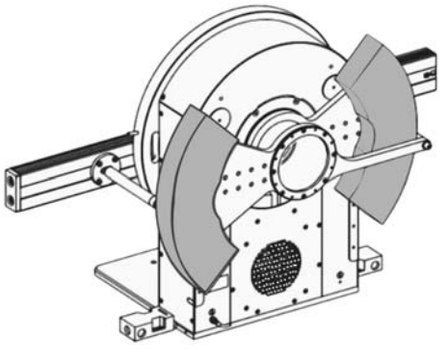

Figure 2.1.10
Example of counterbalancing of a vertical θ–θ goniometer. The counterweights (grey parts) are located at positions matching the weights and locations of the X-ray source and detector. Mounting of different beam-path components with significantly different weight or moving of, for example, the X-ray source and/or the detector to change the respective radii may require repositioning of the counterweights to maintain goniometer accuracy and instrument alignment.

2.1.10 for a goniometer in the ω–θ configuration. Heavy specimen stages may also be supported from below or mounted directly on the bench, disconnected from the goniometer base. However, for heavy beam-path components and larger goniometer radii there is the additional issue of high torques on the incident- and/or the diffracted-beam X-ray optical benches, leading to torsions along the benches. These may significantly deteriorate both the angular accuracy of a goniometer and instrument alignment. For heavy incident-beam-path components such as moving-target X-ray sources, a vertical goniometer base in the ω–2θ configuration is commonly used, as the incident-beam optical X-ray bench is mechanically fixed. For heavy incident- and diffracted-beam-path components a horizontal goniometer base is preferred.

Modern goniometers are equipped with stepping motors and optical encoders, and feature life-span lubrication for maintenance-free operation. The typical accuracy of the two goniometer base axes (ω, 2θ) is of the order of a few thousandths of a degree, with a precision of the order of a few tens of thousandths of a degree. The ψ and φ axes of the specimen stage are mostly used for specimen orientation; the typical angular accuracy and precision are in the range of about 0.01°.

The sphere of confusion of a goniometer is the result of a superposition of all axes and represents the minimum spherical volume covering all possible locations of an infinitely small specimen at all possible orientations. The size of the sphere of confusion depends on issues such as individual axis accuracy and precision, mechanical tolerances, thermal-expansion mismatches, and the weights of the specimen and beam-path components. The sphere of confusion for a two-axis goniometer or a four-axis goniometer with a kappa stage is typically less than 10 μm, and for a four-axis goniometer with a Eulerian cradle less than 50 μm; both values are without a specimen loaded.

Note that the final accuracy of the Bragg angles of the measurement data is mostly determined by instrument alignment, and not by the accuracy specifically of the two goniometer base axes. Optical encoders can measure and control axis positions, but they cannot detect any misaligned or even loose beam-path components. The final data accuracy is determined by the adjustability of an X-ray diffractometer with all its beam-path components. A modern X-ray diffractometer can be aligned to an angular accuracy of equal or better than 0.01° 2θ, which can be checked using suitable standard reference materials (see Chapter 3.1).

2.1.5.3. *Hybrid beam-path systems*

The trend towards multipurpose instrumentation as well as specific application requirements has led to a few specialized goniometer designs. Two major representatives of such designs are (1) multiple-beam-path systems and (2) systems with additional rotational degrees of freedom of beam-path components, such as is required for non-coplanar grazing-incidence diffraction (GID).

2.1.5.3.1. *Multiple-beam-path systems*

Multiple-beam-path systems are usually characterized by integrating more than one beam path on a single goniometer, employing different, complementary beam-path components to meet different application and specimen-property requirements. Mounting two different fixed-target X-ray sources (usually microsources) with different wavelengths (Cu, Mo) is very popular in single-crystal crystallography. Double detector arms are used to mount different types of detectors, most frequently one-dimensional detectors in combination with point detectors. Different X-ray optics can be used to implement different instrument geometries.

A significant driving force behind such multipurpose instrumentation is convenience, *i.e.* to serve a maximum range of applications and specimen types, ideally without the need to manually change the instrument configuration. Indeed, switching between different, preconfigured beam paths may often only require the push of a single software button. However, parallel mounting of different beam-path components raises issues related to the goniometer load and to limitations of angular scan ranges owing to collision issues.

In more recent designs, different X-ray optics have been combined into single motorized modules, allowing switching between different beam paths. Such 'combi-optics' are described in Section 2.1.6.3.4.

2.1.5.3.2. *Non-coplanar beam-path systems*

Non-coplanar (or 'in-plane') grazing-incidence diffraction is a technique for investigating the near-surface region of specimens (ten or fewer nanometres beneath the air–specimen interface). It exploits the high intensity of the total external reflection condition while simultaneously involving Bragg diffraction from planes that are nearly perpendicular to the specimen surface.

As illustrated in Fig. 2.1.11, the incident beam is set at an angle α_I, enabling total external reflection in the coplanar direction (that is coplanar to the diffraction plane); related applications include reflectometry and grazing-incidence small-angle X-ray scattering (GISAXS). 'In-plane' grazing-incidence diffraction

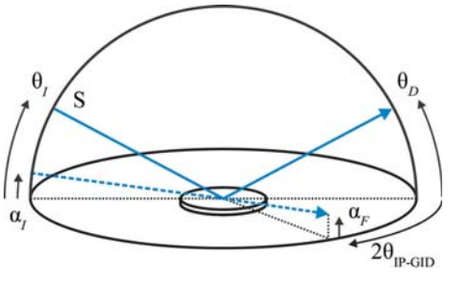

Figure 2.1.11
Illustration of coplanar and in-plane diffraction. S: X-ray source. θ_I, θ_D: incident and diffracted beams for coplanar diffraction. α_I, α_F, $2\theta_{\text{IP-GID}}$: incident-beam angle, exit angle and diffracted-beam angle, respectively, for in-plane grazing-incidence diffraction.

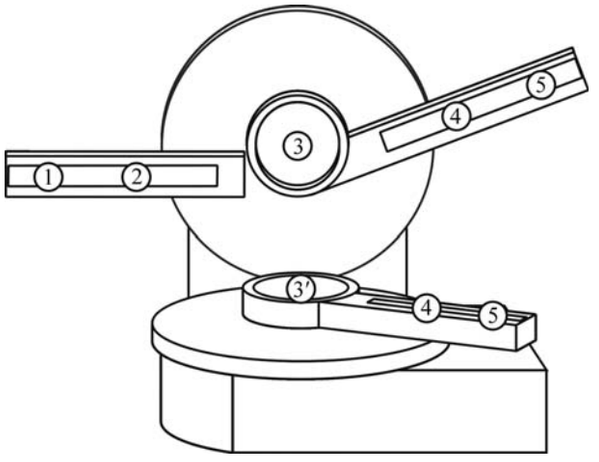

Figure 2.1.12
Sophisticated IP-GID implementation by placing two goniometers vertically with respect to each other, allowing simultaneous coplanar and in-plane measurements using two independent scattered-beam optical X-ray benches (compare with Fig. 2.1.2). The sample stage may be mounted at position 3 or 3′.

(IP-GID) may be measured at angles $2\theta_{\text{IP-GID}}$ in the non-coplanar direction at an exit angle α_F.

There are two principal instrument designs implementing coplanar and in-plane data collection. Firstly, as is obvious from Fig. 2.1.11, a dual-goniometer system may be employed. The most sophisticated implementation has two goniometers placed vertically one above the other, allowing simultaneous coplanar and in-plane measurements using two independent scattered-beam optical X-ray benches as shown in Fig. 2.1.12. Alternatively, the second goniometer may be integrated into the scattered-beam optical X-ray bench, allowing sequential coplanar and in-plane measurements. As a further alternative, a single goniometer may be used, with a Eulerian cradle mounted at the detector position, allowing the detector to be moved around the specimen to perform in-plane measurements. Secondly, a single goniometer equipped with a Eulerian cradle may be used, where the specimen is simply turned by 90° in ψ. As line focus is usually employed for IP-GID measurements, the X-ray source is also turned by 90° to increase the flux.

For all systems, the diffracted-beam optical X-ray benches may be equipped as for multiple beam-path systems, as described in Section 2.1.5.3.1, providing extremely high flexibility. The choice of the most appropriate design depends on issues such as specimen size and weight, the weight of any components in the diffracted-beam path, related spheres of confusion, and the potential need to measure the specimen in a horizontal position.

2.1.6. X-ray sources and optics

This section covers both the generation as well as the conditioning of X-ray beams. All types of X-ray sources, whether laboratory or synchrotron sources, emit a wide range of wavelengths with a characteristic beam divergence and with an intensity related to the power load applied. The function of the incident- and diffracted-beam X-ray optics is to condition the emitted beam in terms of desired wavelength spread, divergence, cross-section size, and shape, and to conserve as much intensity as possible. To achieve maximum performance in terms of intensity and angular resolution, it is essential to design the X-ray optics so that their properties match the characteristics of the X-ray source. Important parameters are the X-ray source beam size and shape, as well as the acceptance angle of the optics given by their design and the distance to the X-ray source.

The optimum choice of an X-ray source and the X-ray optics always depends on the properties of the specimen and the requirements of the applications. Applications requiring high spatial resolution (*e.g.* small single crystals or microdiffraction) or low-angle scattering (*e.g.* thin-film analysis or SAXS) usually require parallel and narrow beams, while diffraction by ideal powders usually works best with larger and slightly divergent beams. As X-ray sources are hardly ever used without X-ray optics, all the components should be seen as one unit determining the beam characteristics at the specimen and eventually at the detector position.

2.1.6.1. *X-ray beam quality measures*

An X-ray beam is characterized by its intensity, wavelength spread, divergence, cross-section size, homogeneity and shape. Simple means for quantifying the quality of an X-ray beam are often useful, and can be used to design an optimal measurement setup by appropriate choice of a combination of X-ray source and X-ray optics. The quantities that are typically used are flux, flux density, brightness and brilliance, all within a 0.1% bandwidth represented by a wavelength range, $\Delta\lambda$, centred around a specific wavelength λ, *i.e.* $\Delta\lambda$ is equal to 1/1000 of λ. While flux, flux density, brightness and brilliance are inter-related, they are distinct and one thus has to consider all of these when comparing X-ray beam characteristics.

Flux represents the integrated intensity of an X-ray beam and is defined as the number of X-ray photons emitted per unit time. The unit for flux is photons per second (p.p.s.).

Flux density is defined as the flux passing through a unit area. The unit is p.p.s. mm^{-2}. Flux density is an appropriate parameter for measuring local counting rates and is synonymous to the term 'intensity' as used in colloquial speech.

Brightness takes the beam divergence into account, and is defined as the flux per unit of solid angle of the radiation cone. The unit is p.p.s. mrad^{-2}. Brightness is an appropriate parameter to use when comparing two X-ray sources with identical focal spot size, as the definition does not contain a unit area.

Brilliance additionally takes the beam dimensions into account and is defined as brightness per mm^2. The unit is p.p.s. mm^{-2} mrad^{-2}. Brilliance is maximized by making the beam size and divergence as small as possible, and the photon flux as large as possible. Two X-ray beams may have the same flux density but different brilliance if the two beams have different beam divergence. Brilliance is thus an appropriate parameter to use when comparing two X-ray sources with different focal spot sizes.

Note that the X-ray source brilliance is an invariant quantity, *i.e.* the brilliance at the specimen position cannot be improved by any optical techniques, but only by increasing the brilliance of the X-ray source. This is a consequence of Liouville's theorem, which states that phase space is conserved. Accordingly, focusing the beam to a smaller size by means of any diffractive or reflective optics will necessarily increase the flux density and the divergence of the X-ray beam, and *vice versa*. Additionally, any diffractive or reflective optics lose flux owing to their reflectivity, which usually is $\leq$90%. Apertures such as slits can help to reduce beam size and divergence, but only at the expense of flux.

Brilliance is more important than flux for experiments with small specimens (*e.g.* single crystals) or small regions of interest (*e.g.* microdiffraction), where it is generally desirable to work

Table 2.1.3
Characteristic wavelengths and absorption edges of metal filters in common use

These data are taken from *International Tables for Crystallography* Vol. C (2004). Metal filters are discussed in Section 2.1.6.3.1.2.

Anode material	$K\alpha_2$	$K\alpha_1$	$K\beta_3$	$K\beta_1$	Metal filter	K absorption edge (Å)
Cr	2.2936510 (30)	2.2897260 (30)	2.0848810 (40)	2.0848810 (40)	V	2.269211 (21)
Co	1.7928350 (10)	1.7889960 (10)	1.6208260 (30)	1.6208260 (30)	Fe	1.7436170 (49)
Cu	1.54442740 (50)	1.54059290 (50)	1.3922340 (60)	1.3922340 (60)	Ni	1.4881401 (36)
Ga†	1.3440260 (40)	1.3401270 (96)	1.208390 (75)	1.207930 (34)		
Mo	0.713607 (12)	0.70931715 (41)	0.632887 (13)	0.632303 (13)	Zr Nb	0.6889591 (31) 0.6531341 (14)
Ag	0.5638131 (26)	0.55942178 (76)	0.4976977 (60)	0.4970817 (60)	Rh Pd	0.5339086 (69) 0.5091212 (42)

† Currently used with dedicated Montel optics only.

with a beam of low divergence and to match the incident beam size to the size of the specimen or the region of interest.

The illumination of larger specimen areas is particularly important for any applications involving polycrystalline specimens, where focusing of the diffracted beam has an advantage over parallel-beam optics in terms of higher beam flux and divergence in that the angular resolution in the diffraction pattern increases. Using an X-ray beam with too small a cross section and/or divergence will result in a smaller or even too small number of diffracting crystallites. This will generally lead to a loss in the diffracted intensity, and may additionally lead to an inhomogeneous intensity distribution in space, leading to random and uncorrectable intensity errors (known as 'particle statistics error', 'spottiness error' or 'granularity error'), and needs to be avoided by all means.

The combination of an appropriate X-ray source with appropriate X-ray optics thus depends on the properties of the specimen and the requirements of the application, and contributes most to the attainable data quality. This is in full agreement with the statement made earlier that there are only a few instrument configurations that will be ideal for any two application areas, or every conceivable sample within a single application area. While changes of most X-ray optics are extremely easy these days, changing between different types of X-ray sources may require significant effort. The choice of the most appropriate X-ray source therefore requires, at the time of instrument acquisition, careful consideration of the types of specimen in relation to the analyses to be conducted.

2.1.6.2. *X-ray sources*

In this section the general concepts of the commonest types of X-ray sources will be described. The physics of X-ray generation and the properties of X-rays have been extensively covered in the literature. More detailed information can be found in, for example, *International Tables for Crystallography* Vol. C (2004) as well as in the textbooks by Pecharsky & Zavalij (2009), Clearfield *et al.* (2008), Jenkins & Snyder (1996), and Klug & Alexander (1974).

2.1.6.2.1. *Generation of X-rays and the X-ray spectrum*

In laboratory X-ray sources, X-rays are produced by a multi-keV electron beam impinging on a metallic target. The X-ray spectrum that is obtained is characterized by a broad band of continuous radiation, accompanied by a number of discrete spectral lines characteristic of the target material. The continuous part of the spectrum ('*Bremsstrahlung*') is generated by the rapid deceleration of the electrons within the target, ranging from lowest energies as a result of gradual deceleration through to a cutoff wavelength whose energy corresponds to the initial kinetic energy of the electron, as a result of instantaneous deceleration. The discrete spectral lines ('characteristic radiation') are the result of electrons knocking out core electrons from the target material. This results in emission of 'fluorescent' X-rays when the perturbed atom relaxes to its ground state by filling up the energy levels of the electrons that have been knocked-out by means of electron transitions from higher electron shells. The energy of the fluorescent radiation is characteristic of the atomic energy levels of the target material. The most commonly used characteristic radiation is that of $K\alpha$, representing the transition of a $2p$ electron (L shell) filling a hole in a $1s$ (K) shell.

The target materials that are commonly in use strongly depend on the application and the type of X-ray source used. The most commonly used target materials range from Cr through to Co, Cu, Mo and Ag. With the recent introduction of liquid-metal targets, see Section 2.1.6.2.2.2(*b*), Ga will find increasing use in applications requiring the smallest spot sizes and highest brilliance. A list of characteristic wavelengths and absorption edges of commonly used metal ($K\beta$) filters is given in Table 2.1.3.

Today's laboratory X-ray sources can be classified as shown in Table 2.1.1, and are described in Section 2.1.6.2.2. For performance considerations see Section 2.1.6.2.3.

2.1.6.2.2. *Types of X-ray sources*

The performance of X-ray sources is usually characterized *via* brilliance as a measure for the quality of the emitted X-rays. The brilliance of an X-ray source is determined by several factors such as electron power density and the take-off angle.

The electron power density is the most important factor. Only a small fraction of <1% of the applied electron energy is converted into X-rays, so most of the incident energy is dissipated within the target as heat. The maximum power density and thus brightness of the X-ray source is limited by the melting or evaporation temperature of solid or liquid metal targets, respectively, and the efficiency with which the heat is removed from the area on which the electrons impact.

The take-off angle describes the angle under which the focal spot is viewed, and typically ranges from 3° to 7°, but may be up to 45°, depending on the type of X-ray source. The actual take-off angle that is chosen represents a compromise. On the one hand, it should be as small as possible to minimize the effectively seen

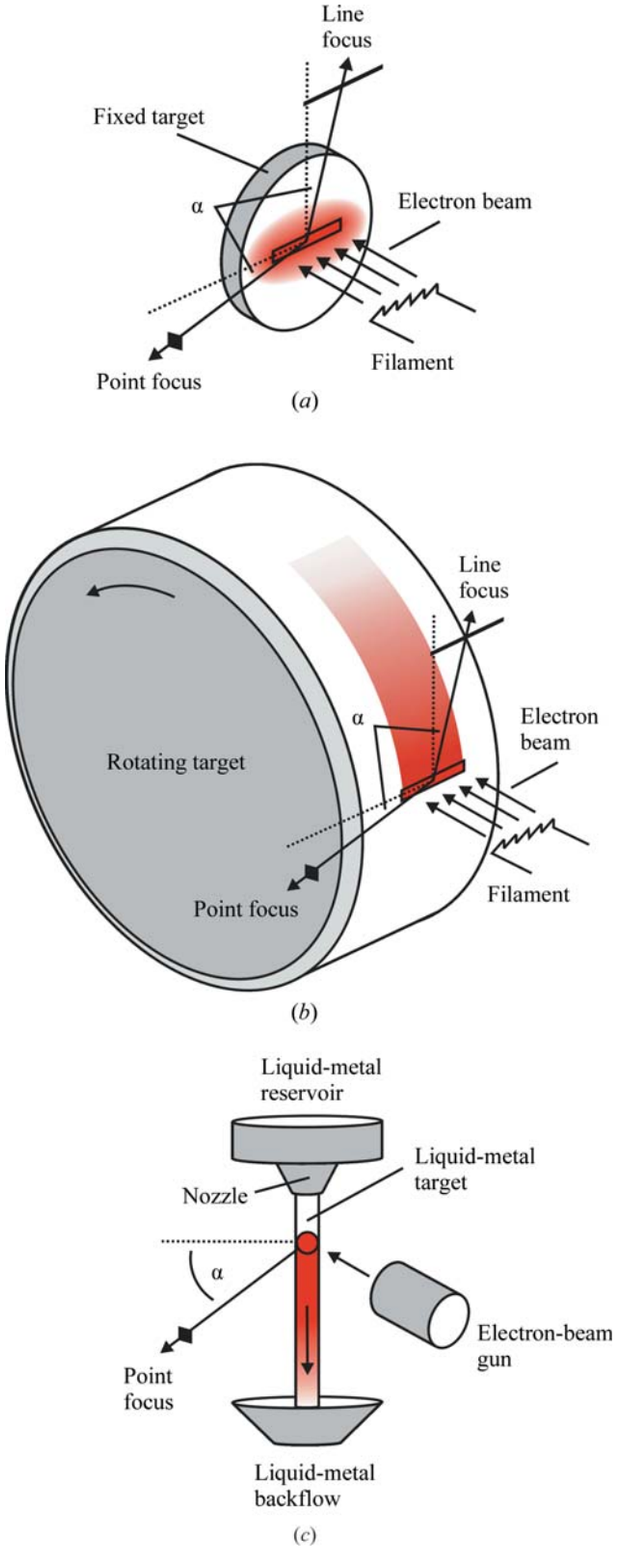

Figure 2.1.13
Illustration of the working principle of laboratory X-ray sources: (*a*) fixed target, (*b*) rotating target, (*c*) liquid-metal jet. α: take-off angle. For fixed targets (*a*) the heat mainly flows towards the cooled back end of the target. For moving targets (*b*, *c*) cold parts of the target are moved into the electron beam continously, providing an extremely large effective cooling efficiency.

width of the focal spot to increase resolution. On the other hand, it cannot be made arbitrarily small to avoid self-absorption by the metal target due to the finite depth in which the X-ray radiation is produced. The higher the tube voltage the larger the take-off angle should be to avoid intensity losses by self-absorption.

In the history of laboratory X-ray source development, most effort has probably been concentrated on techniques for removing the heat from the metal target as efficiently as possible, as illustrated in Fig. 2.1.13, leading to two different categories of X-ray sources for laboratory use: fixed- and moving-target X-ray sources.

2.1.6.2.2.1. Fixed-target X-ray sources

Fixed-target X-ray sources are used in more than 90% of all X-ray diffractometer installations (Fig. 2.1.13*a*). Electrons are generated by heating a filament (cathode) and accelerated towards the metal target (anode) by means of a high potential, typically of the order of 30–60 kV.

In conventional X-ray sources the electrons are focused by an electrostatic lens onto the anode to form the focal spot. Typical power ratings range from several hundred watts up to about 3 kW. The anode is water-cooled from the back. Focal spots are of rectangular shape, and can be viewed at the two long and the two short faces, giving two line and two point foci, respectively. This allows up to four instruments to be operated with a single X-ray source. However, the vast majority of all today's X-ray diffractometers are equipped with an individual X-ray source (and sometimes two, see Section 2.1.5.3.1). This significantly eases alignment as there is no need to align the instrument with respect to the X-ray source, and allows instrument configurations with moving X-ray sources. Modern X-ray-source stage designs allow switching between point and line focus by rotating the X-ray source 90° without alignment and even without the need to disconnect the powder cables and water supply.

Conventional X-ray sources have long and wide electron beams so that a large area of the target is heated (Fig. 2.1.13*a*). The heat generated in the middle of this area can mainly flow in just one direction: towards the water-cooled back of the anode. Heat flow parallel to the surface is minimal, thus limiting the cooling efficiency. It is for this reason that conventional X-ray sources achieve the lowest brilliance of any laboratory X-ray source. Conventional X-ray sources are usually coupled with relatively simple optics and are cheap compared to moving-target systems. In addition they are maintenance-free, apart from periodic changes of the X-ray source owing to ageing.

'Micro-focus' X-ray sources represent another category of X-ray source and are characterized by very small focal spot sizes ranging from a few μm up to about 50 μm. In this type of X-ray source, the improved focusing of the electron beam is achieved by very fine electrostatic or magnetic lenses. Power requirements are significantly less than conventional X-ray sources, ranging from a few watts up to some hundred watts, depending on focal spot size; water cooling is frequently not required. Again, there is no maintenance required beyond periodic tube changes.

As the focal spot area is very small, heat can also flow sideways, improving the thermal cooling efficiency and thus allowing this type of X-ray-source tube to achieve significantly higher brilliance than conventional X-ray sources. To benefit from this increased performance, relatively large optics of the reflective type (see Section 2.1.6.3.3) are required, making micro-focus X-ray source systems significantly more expensive than conventional systems.

The lifetime of a fixed-target X-ray source depends on many factors, of which operation of the source within specifications (such as specific loading and cooling) is particularly important. The 'useful' lifetime may be significantly shorter, even though the X-ray source still operates. Deposition of tungsten from the

filament on the anode and on the inner beryllium window surfaces leads to spectral contamination and substantial loss of intensity with time. Increasing deterioration of the filament may change its position relative to the electrostatic lens used for focusing and result in beam inhomogeneity and additional intensity losses. Further intensity losses and beam inhomogeneity may arise from pitting of the anode surface as a result of the intense electron flux on the anode surface.

2.1.6.2.2.2. *Moving-target X-ray sources*

(*a*) *Rotating-target X-ray sources*. Rotating-target X-ray sources are able to remove heat more efficiently than fixed-target sources, and can thereby sustain higher fluxes of X-ray photons (Fig. 2.1.13*b*). This is achieved by rotating a cooled anode, with a typical diameter ranging from about 10 to 30 cm, at about 6000–12 000 revolutions per minute. The maximum power loads depend on the focal spot size, and can range up to 18 kW for conventional rotating-target X-ray sources, and 3 kW for micro-focus rotating-target X-ray sources. Rotating-target X-ray sources are thus inherently more brilliant, and gain up to an order of magnitude in brilliance compared to their respective fixed-target counterparts.

Rotating-target systems do require routine maintenance such as periodic anode refurbishment and changes of the filament, bearings and seals. The maintenance requirements of micro-focus systems are significantly lower than those of conventional rotating-target systems because of the lower total power loading.

(*b*) *Liquid-metal-jet X-ray sources*. A very recent development is that of liquid-metal-jet micro-focus X-ray sources (Fig. 2.1.13*c*), where a jet of liquid metal acts as the electron-beam target (Hemberg *et al.*, 2003). A thin (<100–225 μm) high-speed (>50 m s^{-1}) liquid-metal jet is injected into vacuum by applying a backing pressure of about 200 bar and is targeted by a focused electron beam with a beam power of up to 200 W and a focal spot size of down to 6 μm. The focal spot is viewed at a take-off angle of about 45° to obtain a symmetric beam usually coupled into Montel optics. (Montel optics are described in Section 2.1.6.3.3.1.)

Ideal materials for use in liquid-jet anodes are electrically conductive to avoid charging and have low vapour pressure to simplify vacuum operation. Among a few materials currently being evaluated, Galinstan (a eutectic mixture of 68.5% Ga, 21.5% In and 10% Sn by weight) is particularly suited for laboratory X-ray analyses, as it is liquid at room temperature (melting point 254 K), with the most intense Ga $K\alpha$ line at 9.25 keV, and less intense In $K\alpha$ and Sn $K\alpha$ lines at 24 and 25.3 keV, respectively.

The obvious advantage of a metal-jet anode is that the maximum electron-beam power density can be significantly increased compared to solid-metal anodes and thus the brilliance can be increased by up to an order of magnitude.

2.1.6.2.3. *Performance of X-ray sources*

The single most important property of an X-ray source is its brilliance, which is proportional to the maximum target loading per unit area of the focal spot, also referred to as the specific loading.

In Table 2.1.4 the maximum target loading and specific loading (relative brilliance) for some typical sealed tubes and some rotating-anode sources with a Cu target are compared. Also listed are data for the liquid-metal jet with Ga as a target. Micro-focus fixed-target X-ray sources have up to two orders of magnitude higher specific loadings compared to conventional fixed target tubes, and even 2 to 5 times higher specific loadings compared to conventional rotating-anode systems. In contrast to fixed-target micro-focus X-ray sources, where the specific loading can only be increased by reducing the source size, moving-target X-ray sources are also made brighter by increasing the speed of the target relative to the electron beam. Moving-target X-ray sources are thus inherently brighter than stationary targets. The liquid-gallium jet has a higher (by a further order of magnitude) specific loading than the most brilliant rotating-anode systems, and now rivals the intensity of second-generation synchrotron beamlines.

Table 2.1.4
Maximum target loading and specific loading for some selected fixed- and moving-target X-ray sources

X-ray source	Focal spot (mm^2)	Maximum load (kW)	Specific loading (kW mm^{-2})
Fixed target			
Broad focus (Cu)	2 × 10	3	0.15
Normal focus (Cu)	1 × 10	2.5	0.25
Long fine focus (Cu)	0.4 × 12	2.2	0.5
Micro-focus (Cu)	0.01–0.05	<0.05	5–50
Moving target			
Rotating anode (Cu)	0.5 × 10 0.3 × 3 0.2 × 2 0.1 × 1	18 5.4 3 1.2	3.6 6 7.5 12
Micro-focus rotating anode (Cu)	0.1	2.7	27
Liquid-metal jet (Ga)	0.02 × 0.02	0.2	>500

2.1.6.3. *X-ray optics*

The purpose of X-ray optical elements is to condition the beam emitted by an X-ray source in terms of desired wavelength spread, divergence, cross-section size and shape, and to conserve as much intensity as possible. X-ray optics currently employed in laboratory X-ray diffractometers may be classified as absorptive, diffractive and reflective, as shown in Table 2.1.1.

Absorptive and diffractive X-ray optics represent selective beam-conditioning techniques, where parts of the beam are eliminated to achieve a particular wavelength distribution and divergence. In contrast to this, reflective optics modify the beam divergence to direct the full beam to the specimen or to the detector. The extremely large number of X-ray optical elements available allows for an enormous range of incident and diffracted beam-path configurations. Choosing the most appropriate X-ray optics and X-ray optics combination for a particular experiment is a challenge for the user. The general rule to be obeyed in order to obtain the best data quality is that the beam dimension, wavelength distribution and divergence should compare to the specimen dimension and angular spread of the structural features to be resolved.

In this section the most common features of X-ray optics in current use will be discussed. A comprehensive survey cannot be given, since there exists an incredible multitude of variants of the basic X-ray optic types listed in Table 2.1.1. X-ray optics have been extensively covered in the literature, for example in *International Tables for Crystallography* Vol. C (2004) and in the textbooks by He (2009), Pecharsky & Zavalij (2009), Paganin

(2006), Fewster (2003), Bowen & Tanner (1998), Jenkins & Snyder (1996), Klug & Alexander (1974), and Peiser *et al.* (1955). An extensive discussion of the principles of combining X-ray optics to optimally suit a wide range of different powder diffraction as well as thin-film applications has been given in the textbook by Fewster (2003).

2.1.6.3.1. *Absorptive X-ray optics*

2.1.6.3.1.1. Apertures

The simplest way of beam conditioning is to place apertures such as slits (line focus) or pinholes (point focus) into the incident and/or diffracted beam to control beam divergence and shape, and to reduce unwanted scattering from air or any beam-path components. Apertures are 'shadow-casting' optics and thus cannot increase flux density. Reducing beam divergence and beam dimensions by means of apertures invariably results in a loss of intensity that is inversely proportional to the slit aperture.

The principles are shown in Fig. 2.1.14. The divergence of a beam is established by the dimensions of the focal spot as well as the aperture and the distance of the aperture from the source (Fig. 2.1.14*a*). The divergence in the diffraction plane is usually called 'equatorial divergence' and the divergence in the axial direction 'axial divergence'. Apertures can be of the plug-in type requiring manual changes of the aperture to obtain different divergence angles, or – usually only for equatorial divergence slits – motorized. Motorized slits are mostly used in the Bragg–Brentano geometry to limit equatorial divergence, which can be arbitrarily chosen and either be kept constant to keep the diffracting specimen volume constant (as is invariably the case with plug-in slits), or varied as a function of 2θ to keep the illuminated specimen length constant. Typical aperture angles range from 0.1–1°.

To provide additional collimation, a second aperture may be placed at some distance away from the first (Fig. 2.1.14*b*). When using the same aperture, an almost-parallel beam may be obtained from a divergent beam at the cost of high intensity losses. A third aperture is often used to reduce scattering by the second slit. In laboratory X-ray diffractometers dedicated for SAXS analysis such collimation systems may reach lengths of more than 1 m.

Another way to parallelize radiation is to use a parallel-plate collimator (PPC), which is manufactured from sets of parallel, equally spaced thin metal plates, as shown in Fig. 2.1.14(*c*). Each pair of neighbouring plates works like a double-aperture arrangement as shown in Fig. 2.1.14(*b*). In contrast to simple slits and pinholes, PPCs do not change the shape of the beam. PPCs arranged parallel to the diffraction plane are usually called 'Soller slits' and are used to control axial divergence. Such devices can be used for focusing as well as parallel-beam geometries with typical aperture angles ranging from 1–5°. Soller slits are usually mounted on both the incident- and diffracted-beam sides of the specimen. PPCs arranged parallel to the diffraction plane are specifically used in parallel-beam geometries to minimize equatorial beam divergence, with typical aperture angles ranging from 0.1–0.5°.

The ways in which the diffracted beam can be conditioned are limited when employing one- or two-dimensional detectors. A particular issue related to these types of detectors is unwanted scattering from air or any beam-path components. Ideally, a closed, evacuated or He-flushed beam path will be used, but this is often not feasible owing to collision issues. For smaller detectors it is possible to place the anti-scatter aperture closer to the specimen surface. Alternatively, a knife edge may be placed on top of the specimen. As knife edges may interfere with divergent beams at higher 2θ angles, it is necessary to move them away from the specimen at higher 2θ angles. Another possibility, limited to one-dimensional detectors, is to use radial Soller slits as shown in Fig. 2.1.14(*d*).

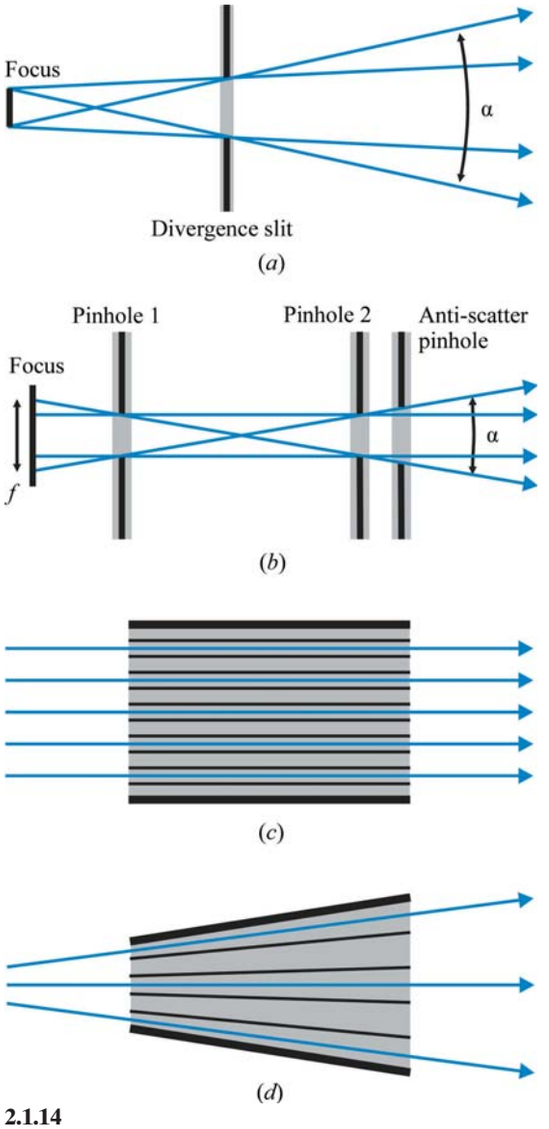

Figure 2.1.14
Apertures used for beam collimation. α: divergence angle, f: virtual focus. (*a*) Single slit or pinhole, (*b*) parallelization through double slits or pinholes, (*c*) parallelization through a parallel-plate collimator, (*d*) a radial plate collimator.

2.1.6.3.1.2. Metal filters

Metal filters are the most frequently used devices for monochromatization of X-rays in laboratory diffractometers. Metal filters represent single-band bandpass devices where monochromatization is based on the K absorption edge of the filter material to selectively allow transmission of the $K\alpha$ characteristic lines while filtering white radiation, $K\beta$ radiation (hence they are frequently known as '$K\beta$ filters'), and other characteristic lines.

A properly selected metal filter has its K absorption edge right between the energies of the $K\alpha$ and $K\beta$ characteristic lines of the source. As a rule of thumb, this is achieved by choosing an element just one atomic number less than the X-ray source target material in the periodic table. For heavy target materials such as

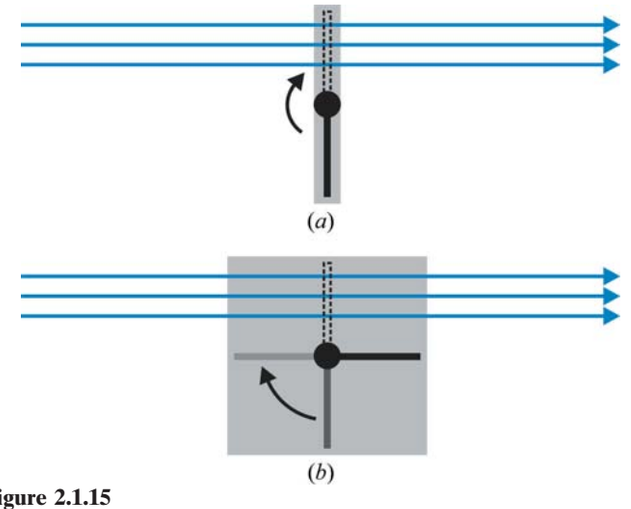

Figure 2.1.15
Motorized switchable (*a*) and rotating (*b*) absorbers.

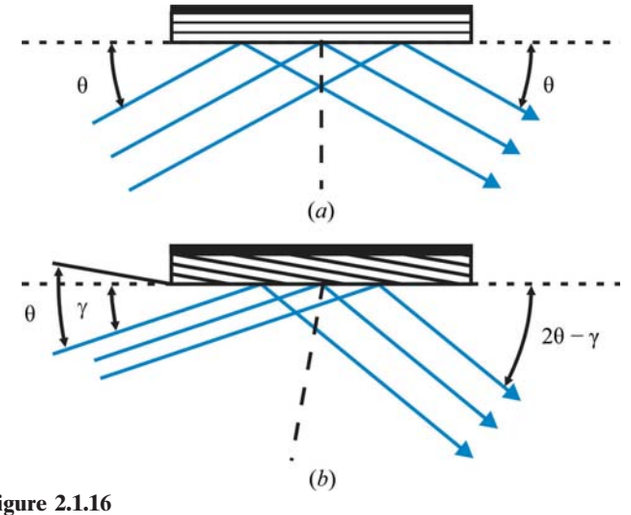

Figure 2.1.16
Illustration of flat single-reflection monochromators. (*a*) Symmetrically cut crystal, (*b*) asymmetrically cut crystal with an angle γ between the reflecting lattice planes and the crystal surface.

Mo or Ag, this rule can be extended to two atomic numbers. A list of metal filters suitable for the most commonly used target materials is given in Table 2.1.3.

A major disadvantage of metal filters is that they cannot completely eliminate $K\beta$ radiation at bearable intensity losses. In addition, they introduce absorption edges at the high-energy (low-angle) side of diffraction peaks, the magnitudes of these being dependent on the wavelength as well as on the filter material and its thickness. While for point detectors absorption edges are usually obscured by counting statistics, they are much more readily visible to position-sensitive detectors owing to the high number of counts that are typically collected.

Positioning of the metal filter does not make a difference in terms of filtering of $K\beta$ or white radiation, but can in the case of specimen fluorescence. Placing the metal filter in the diffracted beam can filter some fluorescence radiation, unless the specimen contains the same element as the metal filter. Taking Cu radiation as an example, most fluorescence radiation excited by Ni in the specimen will pass through a diffracted-beam Ni filter. In this instance, the $K\beta$ filter should be mounted in the incident beam to suppress Cu $K\beta$ radiation, which is very efficient at exciting Ni fluorescence. Balanced-filter techniques, employing two (or more) filters that have absorption edges just above and below $K\alpha$, are no longer in use as the resulting bandpass is still much wider than that of crystal monochromators at even higher intensity losses.

Metal filters are generally supplemented by some energy discrimination by the detector to remove the high-energy white radiation from the X-ray source. The effectiveness of this white-radiation removal depends upon the energy resolution of the detector, and is discussed in Section 2.1.7 for the different detector technologies currently in use. Recent improvements in the energy-discrimination capabilities for silicon strip detectors now even allow filtering of $K\beta$ radiation, completely eliminating the need for metal filters (see Section 2.1.7.2.3.2). As a consequence, the use of metal filters is likely to decline.

Another type of metal filter is represented by absorbers, *e.g.* Cu foils, which are used at high intensities to avoid detector saturation or even damage. Absorbers can be motorized and switched in and out automatically depending on the actual count rates that are detected (Fig. 2.1.15*a*). Several absorbers with different thickness may be combined in the form of motorized rotating absorbers (Fig. 2.1.15*b*).

2.1.6.3.2. *Diffractive X-ray optics*

Single crystals or highly textured polycrystals (mosaic crystals) represent effective beam conditioners by allowing the spectral bandwidth as well as the X-ray beam divergence to be modified. When they are placed at a specific angle with respect to the incident and diffracted beams, according to Bragg's law, only a small spectral bandwidth will be transmitted depending on the divergence of the incident beam and the rocking angle (mosaic spread) of the crystal. Higher harmonics ($\lambda/2$, $\lambda/3, \ldots$) are diffracted as well, but can be successfully suppressed by using materials with small higher-order structure factors and *via* energy discrimination by the detector. Depending on the application, a crystal monochromator can be either used as a spectral filter ('monochromator'), typically used in the incident beam, or as an angular filter ('analyser'), typically used in the diffracted beam to restrict the angular acceptance of the detector.

It is likely that all monochromators currently employed in laboratory X-ray diffractometers are of the reflective type ('Bragg geometry'). Transmission-type monochromators ('Laue geometry') play no role in laboratory powder diffraction. Two designs are in common use and are described below: (*a*) single-reflection monochromators and (*b*) multiple-reflection monochromators.

2.1.6.3.2.1. Single-reflection monochromators

The most common types of single-reflection monochromators are illustrated in Figs. 2.1.16 and 2.1.17. Flat crystals (Fig. 2.1.16) are used in parallel-beam geometry and curved crystals in focusing geometries (Fig. 2.1.17). A beam reflected from a flat crystal with the reflecting lattice planes parallel to its surface (symmetric cut) is nearly parallel (Fig. 2.1.16*a*). If the crystal is cut at an angle to the reflecting lattice planes (asymmetric cut), then the beam will be expanded (Fig. 2.1.16*b*), or compressed if reversed (Fankuchen, 1937). Monochromators can be curved (Johann, 1931) or curved and ground (Johannson, 1933), and may be cut symmetrically (Fig. 2.1.17*a*) or asymmetrically (Fig. 2.1.17*b*). The latter has the particular advantage of providing different focal lengths for the incident and diffracted beam. A shortened incident beam allows the monochromator to be mounted closer to the X-ray source to capture a larger solid angle of the emitted beam. If the diffracted-beam focusing length is

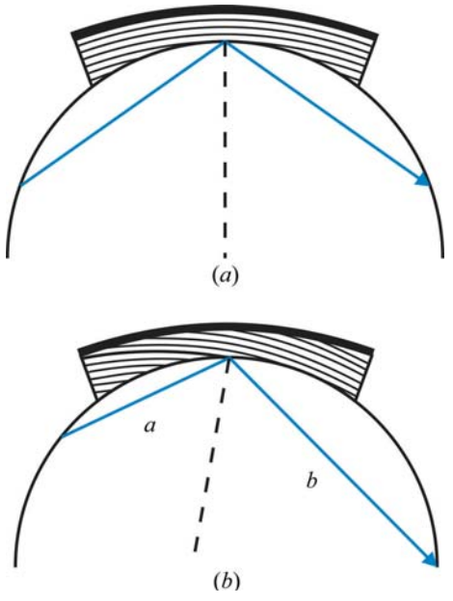

Figure 2.1.17
Illustration of curved and ground single-reflection monochromators. Only the central beam is shown for clarity. (*a*) Symmetrically cut crystal, (*b*) asymmetrically cut crystal with two different focal lengths *a* and *b*.

sufficiently large, then the instrument geometry can be converted between the Bragg–Brentano and the focusing Debye–Scherrer geometries by shifting the monochromator crystal and the X-ray source along the incident-beam X-ray optical bench (see Section 2.1.4.1 and Fig. 2.1.3).

The most commonly used monochromator crystal materials are germanium and quartz, which have very small mosaic spreads and are able to separate the $K\alpha_1/K\alpha_2$ doublet. In contrast to germanium and quartz crystals, graphite and lithium fluoride have large mosaic spreads and thus high reflectivity, but cannot suppress $K\alpha_2$. In principle, any of these monochromators can be mounted in the incident as well as the diffracted beam; the choice mostly depends on the purpose of the monochromator. Germanium and quartz monochromators are typically used as incident-beam monochromators to produce pure $K\alpha_1$ radiation. Graphite (focusing geometries) and lithium fluoride (parallel-beam geometry) are often used as diffracted-beam monochromators to suppress fluorescence radiation. Germanium and quartz can also be used as diffracted-beam monochromators, but are usually not because of their lower reflectivity. Where mounting of diffracted-beam monochromators is difficult or impossible, which is specifically true for one- and two-dimensional detector applications, curved graphite monochromators are frequently used as incident-beam monochromators.

The use of diffracted-beam monochromators – at least in powder X-ray diffraction – is declining steeply because of the geometric incompatibility issues with one- and two-dimensional detector systems (which, since 2010, have been sold with more than 90% of all diffractometers; see Section 2.1.3.2). With the recent improvements of energy-discrimination capabilities for silicon micro-strip detectors, the need for diffracted-beam monochromators will further diminish (see Section 2.1.7.2.3).

2.1.6.3.2.2. Multiple-reflection monochromators

Multiple-reflection monochromators can reduce the wavelength dispersion $\Delta\lambda/\lambda$ significantly more than single-reflection monochromators. Multiple-reflection monochromators are often made of monolithically grooved single crystals and are also known as channel-cut monochromators (Bonse & Hart, 1965). In Fig. 2.1.18 an overview is given of the most common channel-cut monochromator types; for a detailed discussion see *e.g.* Hart (1971) and Bowen & Tanner (1998). Successive reflection of the X-ray beam at the channel walls by the same lattice planes causes a strong reduction of the X-ray intensity contained in the tails of the beam. Depending on the number of reflections, multiple-reflection monochromators are denoted as two-bounce, three-bounce *etc*. channel-cut monochromators. The Bartels monochromator (Bartels, 1983) comprises two two-bounce channel-cut crystals. For Cu radiation, such a monochromator results in a wavelength spread which is less than the natural line width of the Cu $K\alpha_1$ line. The most commonly used crystal material is germanium, which delivers higher intensity than silicon, using the 400, 220, or 440 reflections. Crystals may be cut symmetrically or asymmetrically. In Table 2.1.5 several types of

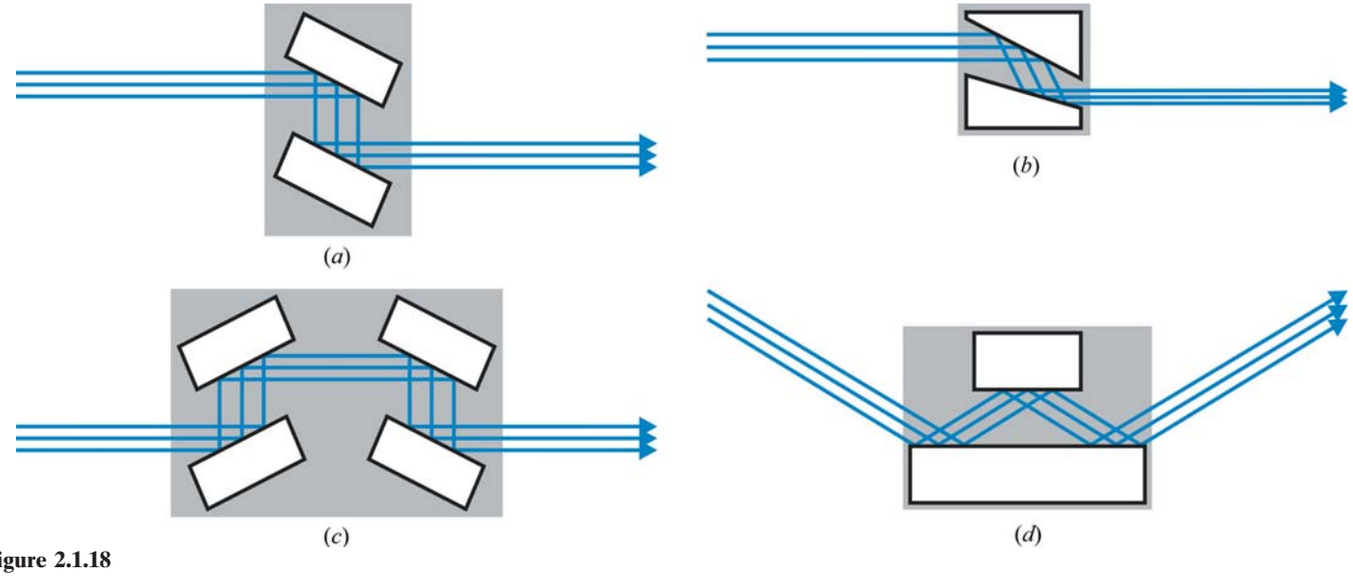

Figure 2.1.18
Illustration of multiple-reflection monochromators. (*a*) Symmetrically cut two-bounce channel-cut monochromator, (*b*) asymmetrically cut two-bounce channel-cut monochromator for beam compression, or, if reversed, for beam expansion, (*c*) symmetrically or asymmetrically cut four-bounce channel-cut monochromator, (*d*) symmetrically cut three-bounce channel-cut monochromator.

Table 2.1.5
Comparison of divergence and intensity for several types of germanium channel-cut monochromators

In each case, the monochromator is coupled with a graded multilayer providing 3×10^9 counts per second at <0.028° beam divergence. The values in parentheses denote the percentage of intensity diffracted by the respective monochromator crystals.

Type	(*hkl*)	Divergence (°)	Intensity
Two-bounce	220, symmetric	<0.0052	5.0×10^7 (∼1.5%)
Two-bounce	220, asymmetric	<0.0085	3.3×10^8 (∼10%)
Two-bounce	400, asymmetric	<0.0045	4.8×10^7 (∼1.5%)
Four-bounce	220, symmetric	<0.0035	6.5×10^6 (∼0.2%)
Four-bounce	220, asymmetric	<0.0080	2.7×10^7 (∼1%)
Four-bounce	440, symmetric	<0.0015	2.2×10^5 (∼0.075%)

germanium channel-cut monochromators are compared in terms of divergence and intensity.

Switching between different channel-cut monochromators is extremely easy these days and can be accomplished without the need for any tools and without realignment. This is also true for cases where a beam offset is introduced, *e.g.* by switching between two- and four-bounce channel-cut monochromators. In sophisticated instruments such an offset can be compensated fully automatically by a software-controlled motor.

The combination of different types of channel-cut monochromators in both the incident and diffracted beam allows the construction of advanced diffractometer configurations with extremely high resolution capabilities. It should be emphasized that laboratory X-ray diffractometers can have identical optical configurations to diffractometers operated at synchrotron beamlines. The important and obvious difference, however, is the extremely low flux coming from laboratory X-ray sources, which is further diminished by each reflection in a channel-cut monochromator (Table 2.1.5). While such configurations work perfectly for strongly scattering single-crystal layers in thin films, for example, analysis of ideal powders is normally not possible.

2.1.6.3.3. *Reflective X-ray optics*

2.1.6.3.3.1. Multilayer mirrors

Multilayer mirrors used in laboratory X-ray diffractometers are efficient beam conditioners, using total reflection as well as Bragg reflection on inner interfaces of a multilayer structure to modify beam divergence, cross-section size, shape and – to some extent – spectral bandwidth. A comprehensive description of current mirror designs and important mirror properties is found in the VDI/VDE Guideline 5575 Part 4 (2011).

Multilayer mirrors consist of a multilayer coating deposited on a flat or curved substrate. The *imaging* characteristics are mostly determined by the contour of the mirror surface as defined by the substrate surface. The most common contours include planes, ellipsoids, paraboloids, elliptic cylinders or parabolic cylinders. The *spectral reflection* properties are determined by the coating, which may consist of some 10 up to 1000 alternating layers of amorphous low-density ('spacer') and high-density ('reflector') materials, with a period of a few nanometres. The first curved mirrors were produced by depositing the multilayers on a flat substrate that was subsequently bent to the desired contour, yielding typical r.m.s. slope errors of about 15 arcsec. By using prefigured substrates with r.m.s. slope errors below 1.7 arcsec, significantly improved reflectivity and lower beam divergence are obtained. Laterally graded multilayer mirrors (so-called 'Göbel mirrors') have a layer thickness gradient parallel to the surface

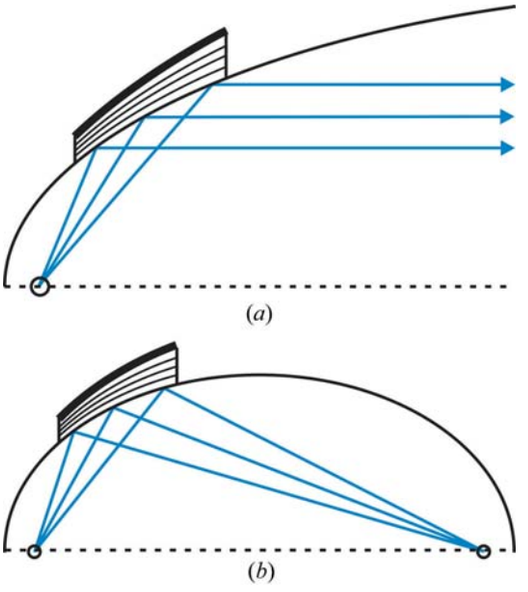

Figure 2.1.19
Schematic of graded multilayer mirrors. (*a*) Parabolic mirror for parallelization of a divergent beam, or, if reversed, focusing of a parallel beam. In the latter case the mirror will also filter some specimen fluorescence. (*b*) Elliptical mirror for focusing of a divergent beam.

(Schuster & Göbel, 1996), which, when combined with a planar, parabolic or elliptic substrate contour, produce a divergent, parallel or focusing beam. Fig. 2.1.19 illustrates graded multilayer mirrors for parallelization and focusing in the plane of diffraction.

For beam conditioning in two perpendicular directions, two perpendicularly oriented curved mirrors may be used, as illustrated in Fig. 2.1.20. In the Kirkpatrick–Baez scheme (Kirkpatrick & Baez, 1948), two mirrors are cross-coupled as shown in Fig. 2.1.20(*a*). This setup has some issues related to the inherently different capture angles and magnification of both mirrors, resulting in less flux from smaller sources and in different divergences in both directions for elliptical mirrors. The Montel optics (Montel, 1957) shown in Fig. 2.1.20(*b*) overcome these issues by arranging both mirrors in a 'side-by-side' configuration.

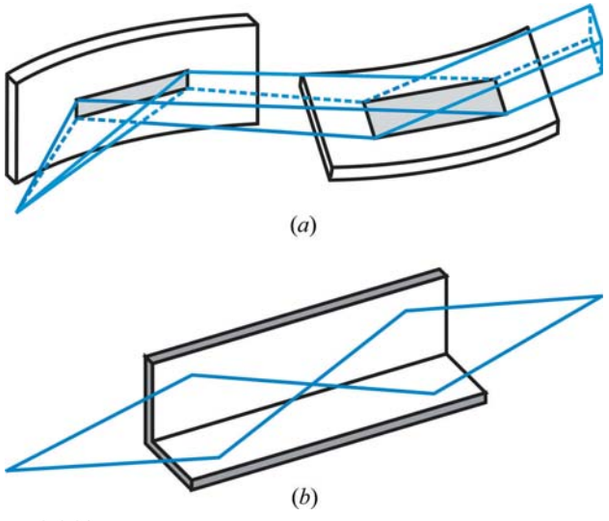

Figure 2.1.20
Examples for orthogonally positioned curved mirrors for beam conditioning. (*a*) Kirkpatrick–Baez scheme employing two parabolic mirrors to create a parallel beam, (*b*) Montel optics employing two elliptical mirrors side-by-side to create a focusing beam.

Mirrors are available for all characteristic wavelengths used in laboratory X-ray powder diffractometers. A wealth of different materials are being used as double layers (reflector/spacer), including but not limited to W/Si, W/B_4C, Ni/C, Ru/B_4C, Ti/B_4C, V/B_4C, Cr/B_4C and Mo/B_4C. The double-layer materials may be selected according to the energies of their absorption edges to make the mirror act as a filter as well. While none of these mirrors is strictly speaking a monochromator, appropriate selection of the double-layer materials, depending on the wavelength used, will allow monochromatization of the radiation to $K\alpha$ while $K\beta$ and *Bremsstrahlung* are suppressed.

Within the past two decades mirror systems have become invaluable for all applications requiring a small and/or highly parallel beam. In particular, coupling of a parallel-beam mirror with multiple-reflection channel-cut monochromators allows the use of a wider solid-angle range of the X-ray source and a gain of nearly two orders of magnitude in intensity (Schuster & Göbel, 1995). For applications requiring ideal powders, however, too-small as well as too-parallel beams may result in too small a number of diffracting crystallites, which will generally reduce the diffracted intensity, and may additionally lead to particle statistics errors (see also Section 2.1.6.1).

Today, advanced sputtering techniques allow the fabrication of a wealth of different multilayer optics with virtually arbitrary beam divergences to generate focusing, parallel and divergent beams, for both point- and line-focus applications. The most comprehensive overview of currently available mirrors and up-to-date specifications will be found in manufacturers' brochures.

2.1.6.3.3.2. Capillaries

X-ray capillary optics are finding increasing use in applications where a small focused beam with high intensity is required. Their design, important properties and applications are discussed by *e.g.* Bilderback (2003), He (2009), and the VDI/VDE Guideline 5575 Part 3 (2011).

X-ray capillary optics employ total external reflection by the inner surface of hollow glass tubes to guide and shape X-ray radiation. For incidence angles lower than the critical angle of total reflection the X-ray radiation is guided through the optics at very low losses. The transmission efficiency depends upon the X-ray energy, the capillary materials, reflection surface smoothness, the number of reflections, the capillary inner diameter and the incident beam divergence, and is thus determined by the particular design of the given optics. Generally, the transmission efficiency decreases with increasing X-ray energy owing to the decreasing critical angle of total reflection. The role of X-ray capillary optics as energy filters is insignificant, therefore capillaries are usually used in combination with monochromatization

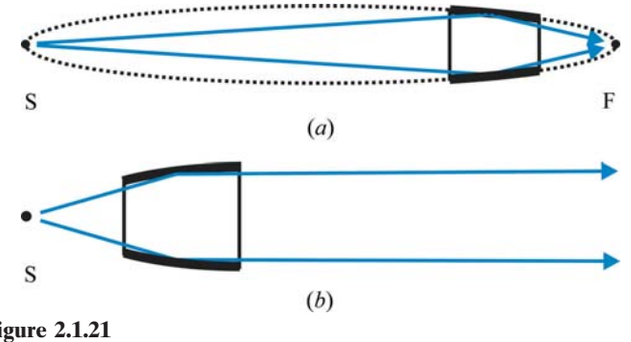

Figure 2.1.21
Schematic of monocapillary optics. (*a*) Elliptical and (*b*) parabolic monocapillary. S = source; F = focal point.

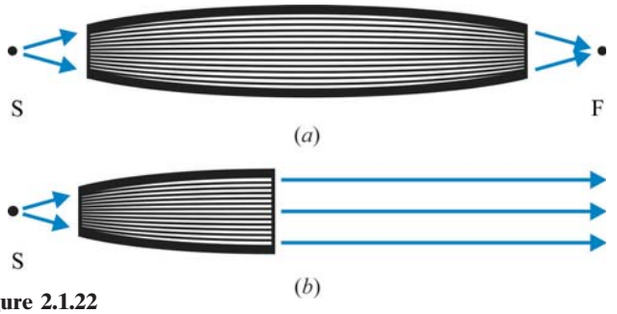

Figure 2.1.22
Schematic of polycapillary optics. (*a*) Focusing and (*b*) parallel-beam polycapillary. S = source; F = focal point.

devices such as metal filters, incident-beam graphite monochromators or graded multilayers. Gains in flux density of more than two orders of magnitude compared to pinhole systems have been reported. The most common X-ray capillary optics currently used in laboratory X-ray powder diffractometers can be categorized as either monocapillaries or polycapillaries.

Monocapillaries consist of ellipsoidal or paraboloidal capillaries for focusing or parallelizing X-rays by means of single or multiple total reflections, as illustrated in Fig. 2.1.21. The exit-beam divergence is controlled by the capillary diameter and length as well as the critical angle of total reflection; typical spot sizes range from some 20 mm down to less than 1 µm. Single-reflection monocapillaries are achromatic and almost 100% efficient. Their most important limitations are figure slope errors limiting the spot size. Multi-reflection monocapillaries can have the smallest spot sizes, which do not depend on the source size. An important drawback is that the beam is smallest at the capillary tip. In order to obtain the smallest possible spot size the sample has to be positioned to within 10–100 times the diameter of the tip exit size, *e.g.* 10–100 µm for a capillary with a 1 µm tip exit size.

Polycapillaries (*e.g.* Kumakhov & Komarov, 1990) are monolithic systems of micro-structured glass consisting of thousands up to several millions of channels, which are tapered at one or both ends to form desired beam profiles as illustrated in Fig. 2.1.22. A single channel can efficiently turn an 8 keV beam by up to 30° by multiple total reflections. Polycapillaries can collect a very large solid angle up to 20°, resulting in very high intensity gains. Typical spot sizes range from some 20 mm down to about 10 µm and are energy dependent, getting larger at lower energies.

2.1.6.3.4. *Combi-optics*

The steadily growing trend towards multipurpose instrumentation has led to a multitude of X-ray optics combined in single modules to eliminate reassembling and realignment. Such 'combi-optics' are usually motorized and allow a fully automatic, software-controlled switch between different beam paths to switch between different instrument geometries or to optimize beam conditioning (*e.g.* high flux *versus* high resolution).

A frequent requirement is the ability to switch between the divergent-beam Bragg–Brentano and parallel-beam Debye–Scherrer geometries, which can be achieved by two combi-optics as illustrated in Fig. 2.1.23. In this example, the incident-beam combi-optics consist of a variable slit and a Göbel mirror. When operating as a variable slit (Fig. 2.1.23*a*), the parallel-beam path is blocked by the variable slit. Turning the variable slit parallel to the divergent beam (Fig. 2.1.23*b*) enables the parallel beam and blocks the divergent beam. The diffracted-beam combi-optics consist of a set of two parallel-plate collimators, which are

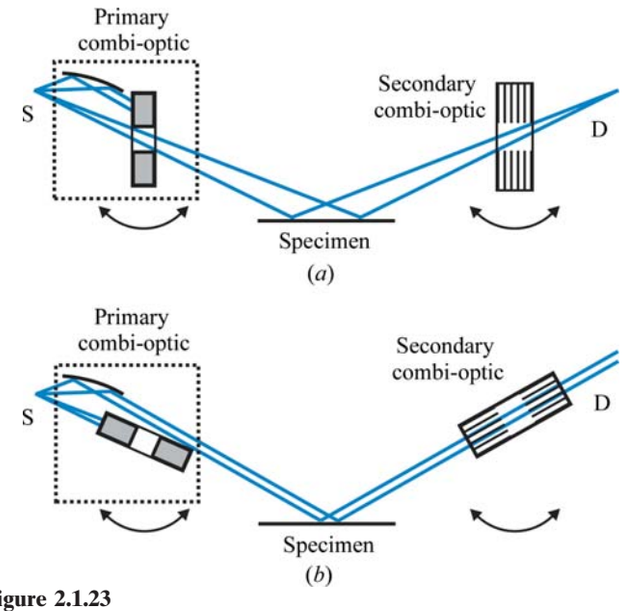

Figure 2.1.23
Incident and diffracted beam combi-optics for switching between (*a*) the Bragg–Brentano geometry and (*b*) the parallel-beam geometry. S: X-ray source; D: detector.

separated by a small gap. When turning the two parallel-plate collimators into the beam direction, only those diffracted rays running parallel to the collimator plates will reach the detector (Fig. 2.1.23*b*). When turning the collimators by approximately 90°, the gap between the two collimators acts as a variable slit enabling a divergent beam (Fig. 2.1.23*a*).

Significantly more sophisticated combi-optics are used in X-ray diffractometers that are mostly used for thin-film analysis. In Fig. 2.1.24 an example for two different incident-beam and four different diffracted-beam paths is shown, providing the choice between eight different beam paths depending on the properties of the specimen and the application requirements. The incident beam path is characterized by a fixed-target X-ray source equipped with a Göbel mirror, attached on a motorized mount. By rotating this arrangement by about 5°, the beam travels either through a rotary absorber followed by a two-bounce channel-cut monochromator and a slit (upper beam path, high-resolution setting), or just through a single slit (lower beam path, high-flux setting). The diffracted beam path represents a double-detector setup, typically consisting of a point detector (D1) and a position-sensitive detector (D2). For the point detector three different beam paths can be chosen by means of a switchable slit, which either sends the beam through a three-bounce channel-cut analyser, or through the same two-parallel-plate-collimator arrangement already discussed in Fig. 2.1.23, either acting as a parallel-plate collimator or a variable slit. A fourth beam path without any diffracted-beam X-ray optics allows use of the position-sensitive detector.

2.1.7. X-ray detectors

The general concepts of X-ray detectors are described here with the focus on practical aspects. The physics of X-ray detection and the individual detector technologies are extensively covered in the literature. He (2009) gives a comprehensive discussion that also includes the most recent detector technologies. Additional detailed descriptions are found in *International Tables for Crystallography* Vol. C (2004), as well as in the textbooks by Pecharsky & Zavalij (2009), Clearfield *et al.* (2008), Paganin (2006), Jenkins & Snyder (1996), and Klug & Alexander (1974).

2.1.7.1. *Detector parameters*

There are many ways to characterize the properties and performance of an X-ray detector.

Ideally, in a given detector operated under appropriate conditions, (1) each photon will produce a detectable signal and (2) the signal recorded is proportional to the number of photons detected. If both conditions are fulfilled then the detector has unit *quantum efficiency*. The *detective quantum efficiency* (DQE) may be defined as the squared ratio of the output signal-to-noise ratio to the input signal-to-noise ratio, expressed as a percentage. A detector's DQE is generally less than 100% because there is always detector noise and not every photon is detected. The DQE thus depends on the characteristics of the detector (*e.g.* transmission of the detector window, count rates and dead time, *etc*.) and varies with the X-ray energy for the same detector.

The *detector linearity* determines the accuracy of intensity measurements and depends on the ratio between the photon

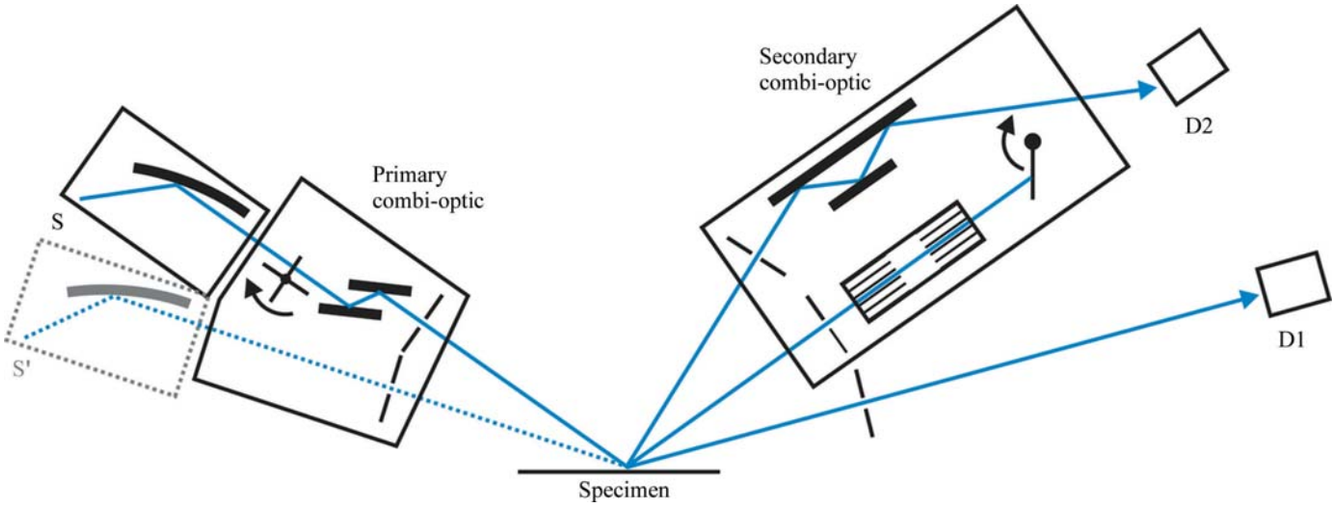

Figure 2.1.24
Example of the use of highly sophisticated incident- and diffracted-beam combi-optics in combination with a rotatable X-ray source and a double detector arm. This setup enables two different incident-beam and four different diffracted-beam paths, and thus provides a choice between eight different beam paths, depending on the properties of the specimen and the requirements of the application. S: X-ray source, S′: X-ray source rotated by about 5°, D1, D2: detectors.

count rate and the rate of signals generated and registered by the detector. In any detector it takes some time to process the conversion of an individual photon to a voltage pulse, which is related to the detector *dead time*: photons arriving while the detector is still processing the previous photon conversion may be lost. The detector dead time is related to the physical characteristics of the detector, *e.g.* the drift time in a gas-ionization detector, or the read-out time of the counting electronics, *e.g.* the shaping time of the amplifier. The effect of dead time becomes a substantial issue at high photon count rates, when the dead time becomes a significant part of the average time separation between two arriving photons, leading to increasing intensity losses at higher count rates. Detectors can be categorized as being non-paralysable or paralysable with respect to dead time. A non-paralysable detector is dead for a fixed time after each count, but not influenced by photons arriving during the dead time. Counting losses increase with increasing count rates, but the true count rate of a nonparalysable detector can be corrected unless the maximum observed count rate is equal to the inverse of the dead time. In a paralysable detector, a second photon arriving within the dead time can not be counted but will extend the dead time up to a point where the detector will be incapable of collecting any counts at all (saturation point). Modern detectors can stand the count rates obtained in powder diffraction experiments using fixed-target X-ray sources. At very high count rates, *e.g.* those obtained in thin-film experiments such as reflectometry, it may be necessary to attenuate the beam. Sophisticated instruments are equipped with an electronic feedback system and automatic absorbers (see Section 2.1.6.3.1.2) to ensure that detector saturation is avoided.

The *dynamic range* of a detector may be defined as the range between the smallest detectable photon count rates (determined by inherent detector noise such as readout and dark noise) to the largest acceptable photon count rates (determined by the dead time).

Energy resolution is the ability of a detector to resolve two photons that have different energies. Energy resolution is typically characterized by the size of the detector energy window, ΔE, in electron volts, as determined by the full width at half maximum (FWHM) of the detector-efficiency curve as a function of energy, with the detector and counting electronics set to a specific wavelength. Another frequently used expression for energy resolution is the ratio of the detector energy window size to the energy of the monochromatic X-ray beam, E, expressed as $\Delta E/E$.

The *proportionality* of the detector determines how the size of the generated voltage pulse is related to the energy of the absorbed X-ray photons, and electronic methods (pulse-height selection) can be used to discriminate between different energies. An accurate proportionality thus allows the use of *energy discrimination* as a form of monochromatization, where the energy is filtered by the detector rather than by an optical element such as a metal filter, crystal or mirror; see Section 2.1.6.3. Signals corresponding to photons with too high or too low energies are discarded.

The size and weight of detectors may impose several practical constraints, see also Section 2.1.4.2. For large detectors the accessible angular range may be limited owing to collision issues. For heavy detectors a horizontal goniometer may be preferred over a vertical goniometer (unless horizontal specimen positioning is imperative) in order to minimize the goniometer load.

X-ray detectors may be broadly classified as *counting detectors* or *integrating detectors*. Counting (digital) detectors are able to detect and count individual photons. The number of pulses counted per unit time is proportional to the incident X-ray flux. Integrating (or analogue) detectors accumulate photon-induced signals for a given period of time, prior to the integrated signal being read out and converted into an (analogue) electrical signal. The signal size is proportional to the flux density of the incident X-rays.

Counting and integrating detectors each have their clear advantages and disadvantages. Counting detectors normally have a greater dynamic range than integrating detectors, while integrating detectors normally have better spatial resolution (Section 2.1.7.3). Energy resolution is only possible for counting detectors. Readout and dark noise are usually higher for integrating detectors. Integrating detectors are not limited by the photon count rate as there is no dead time; nevertheless, the measurement time has to be kept sufficiently small to avoid saturation.

2.1.7.2. *Detector types*

Counting and integrating detectors can be further distinguished by their working principle, and are represented by scintillation, gas-ionization and semiconductor detectors. The most commonly used detector types and their properties are listed in Tables 2.1.1 and 2.1.6, respectively.

At the end of the 1990s the types of detectors in use were scintillation, gas-ionization, Si(Li) and image-plate detectors, with the scintillation counter being the most common by far. Usage of photographic film had already greatly diminished by that time. With the introduction of a series of new one- and two-dimensional detector technologies since the late 1990s, the X-ray detection landscape changed completely. New semiconductor-based detectors (silicon micro-strip, silicon pixel) as well as gas-ionization-based detectors (micro-gap) reached a market share of >90% in newly sold X-ray powder diffractometers within only a few years. As a consequence, classical metal-wire-based proportional counters and scintillation counters will probably become obsolete before 2020. The same is expected for CCD-based detectors, which will be replaced by the very recently introduced complementary metal–oxide–semiconductor (CMOS) active pixel sensor technology.

In the following the working principles of currently available detector types will be briefly described. Matters that are specific to zero- (0D), one- (1D) and two-dimensional (2D) detection are discussed in Section 2.1.7.3. While image plates are still in use, their market share in newly sold systems has become insignificant. Photographic film techniques are totally obsolete. For these reasons, these two detector types will not be taken into further consideration.

2.1.7.2.1. *Scintillation counters*

Scintillation counters are constructed from a scintillator crystal optically coupled to a photomultiplier tube. The crystal is typically made of sodium iodide (NaI) doped with about 1% thallium, frequently denoted as NaI(Tl). When irradiated by X-ray radiation, blue light (∼415 nm) is emitted and converted to electrons in a photomultiplier and amplified; the resulting pulses are registered as photon counts.

The height of the outgoing pulses is proportional to the energy of the incoming X-ray photons. This permits the use of pulse-height selection but only allows for poor energy resolution. The relatively high count rate and a moderate noise level result in a moderate dynamic range. These characteristics are the reason for the formerly wide-ranging acceptance of the scintillation counter

Table 2.1.6
Important detector properties at 8 keV as reported by various vendors

Only typical values are given to allow approximate comparisons. Detector properties strongly depend on individual detector designs and are subject to high development rates.

		Gas ionization (Xe/CO_2 gas filling)		
	Scintillation	Wire based (0D)	Wire based (1D/2D)	Micro-gap (1D/2D)
DQE	∼95%	∼95%	∼80%	∼80%
Dynamic range	$>6 \times 10^6$	$>10^6$	$>10^4$ (1D) $>10^6$ (2D)	$>8 \times 10^7$ (1D) $>10^9$ (2D)
Maximum global count rate	$>2 \times 10^6$ c.p.s.	$>7.5 \times 10^5$	$>10^5$ (1D) $>4 \times 10^4$ c.p.s. (2D)	$>8 \times 10^5$ (1D) $>1.6 \times 10^6$ c.p.s. (2D)
Maximum local count rate	n/a	n/a	$>10^4$ (1D) $>10^4$ c.p.s. mm^{-2} (2D)	$>9 \times 10^5$ c.p.s. mm^{-2} (1D, 2D)
Noise	∼0.3 c.p.s.	∼1 c.p.s.	∼1 c.p.s. (1D) $<5 \times 10^{-4}$ c.p.s. mm^{-2} (2D)	<0.01 c.p.s. (1D) $<5 \times 10^{-4}$ c.p.s. mm^{-2} (2D)
Energy resolution	∼3500 eV (∼45%)	∼1600 eV (∼20%)	∼1600 eV (∼20%)	∼1600 eV (∼20%)
Detection mode	Photon counting	Photon counting	Photon counting	Photon counting

	Semiconductor				
	Si(Li)	Strip	Pixel	CCD	CMOS
DQE	>98%	>98%	>98%	∼20–60%	∼75%
Dynamic range	$>10^6$	$>7 \times 10^6$ per strip	$>10^9$	$>5 \times 10^4$	$>1.6 \times 10^4$
Maximum global count rate	$>10^5$ c.p.s.	$>10^8$ c.p.s	$>10^7$ c.p.s. mm^{-2}	n/a	n/a
Maximum local count rate	n/a	$>7 \times 10^5$ c.p.s. per strip	$>10^4$ per pixel	n/a	n/a
Noise	∼0.1 c.p.s.	∼0.1 c.p.s. per strip	$\sim 2.5 \times 10^{-3}$ c.p.s. mm^{-2}	<0.1 c.p.s. per pixel	<0.05 c.p.s. per pixel
Energy resolution	∼200 eV (∼4%)	∼1600 eV (∼20%)†	>1000 eV (∼12.5%)	n/a‡	n/a
Detection mode	Photon counting	Photon counting	Photon counting	Integrating§	Integrating

† ∼380 eV/∼5%; Wiacek *et al.* (2015). ‡ >300 eV/>6% in photon-counting mode, see text. § Photon-counting mode possible, see text.

as the detector of choice. An important disadvantage these days is the limitation to 0D detection.

2.1.7.2.2. *Gas-ionization detectors*

The gas-ionization detectors in current use are proportional counters and can be of the 0D, 1D or 2D detection type. Common to all proportional counters is a gas-filled chamber permeated by a non-uniform electric field between positive and negative electrodes, held at a constant potential difference relative to each other. Typically the noble gases Ar or Xe are used as gas fill, mixed with a small amount of quenching gas such as CH_4 or CO_2 to limit discharges. When an X-ray photon travels through the gas-filled volume, it may be absorbed by a noble-gas atom, resulting in the ejection of an electron (photoelectric and Compton recoil). This electron, accelerated by the electric field towards the anode, will cause an avalanche by subsequent ionization along its path (gas amplification), generating an electric pulse which can be registered. The height of the generated pulse is proportional to the energy of the incoming X-ray photon and permits the use of pulse-height selection to achieve moderate energy resolution.

2.1.7.2.2.1. Wire-based proportional counters

In a point proportional detector (0D detection), the pulses generated are measured at one end of a wire (or a knife edge). Position-sensitive (1D and 2D detection) proportional detectors have the added capability of detecting the location of an X-ray photon absorption event. In a 1D proportional detector, pulses are detected at both ends of the wire. Thus the time difference between the measurements of a given pulse can be used to determine the location of the discharge. 2D proportional counters consist of three arrays of wires (multiwire proportional counter, MWPC; Sauli, 1977; Charpak *et al.*, 1968), where one array forming the anode plane is placed between two cathode arrays with their wires oriented parallel and orthogonal to the anode-plane wires, respectively.

Low count rates and low-to-moderate detector noise result in low-to-moderate dynamic ranges. Wire-based proportional counters are not competitive with micro-gap and semiconductor detectors, as can be seen in Table 2.1.6, and are therefore being driven out of the market.

2.1.7.2.2.2. Micro-gap detectors

The maximum count rates in 'classical' metal-wire-based proportional counters are severely limited by the long ion-drift times in the chamber (which typically have a cathode to anode spacing of ∼10 mm). This issue has been successfully addressed by so-called micro-gap technology using parallel-plate avalanche chambers with a readout electrode separated from a resistive anode. The key feature is the resistive anode, which allows a very small amplification gap (1–2 mm cathode to anode spacing) at an increased average electric field intensity, while preventing discharges (Durst *et al.*, 2003; Khazins *et al.*, 2004). As a result, micro-gap detectors can achieve count rates several orders of magnitude higher than classical proportional counters at higher position sensitivity. Micro-gap detectors of the 1D and 2D detection type are available. Moderate count rates and very small

noise levels result in very high dynamic ranges. Notably, in contrast to wire detectors, micro-gap detectors are not likely to be damaged by accidental exposure to a high-intensity direct beam, as a patterned anode plane is used rather than wires.

2.1.7.2.3. *Semiconductor detectors*

Semiconductor (or solid-state) detectors are solid-state ionization devices in which electron–hole pairs instead of electron–ion pairs are generated by incoming photons, and they are sensitive to the entire electromagnetic spectrum from visible light to X-rays. The energy required for production of an electron–hole pair is very low compared to the energy required for production of paired ions in a noble-gas-filled detector. As a consequence, a larger number of charge pairs with a smaller statistical variation are generated in semiconductor detectors, resulting in intrinsically higher energy-resolution capabilities. The efficiency of semiconductor detectors is very high due to the high absorption of the semiconductor materials, usually reaching 100%, but may decline at higher photon energies if the photons are not fully absorbed in the semiconductor *e.g.* because of insufficient thickness.

2.1.7.2.3.1. The Si(Li) detector

The Si(Li) detector sensor consists of a lithium-drifted silicon crystal which must be cooled to prevent lithium diffusion and to reduce dark noise. An important advantage of this detector is its excellent energy resolution of even better than 200 eV (4%) at 8 keV (Cu radiation), allowing very effective filtering of Kβ and fluorescence radiation and thus operation without a metal filter or a diffracted-beam monochromator. As Peltier cooling is sufficient, the Si(Li) detector type has found wide interest for applications benefitting from high energy resolution, unlike energy-dispersive detectors requiring operation under cryogenic conditions [*e.g.* Ge(Li)]. In particular, the Si(Li) detector significantly extends the application range of today's X-ray diffractometers by allowing energy-dispersive X-ray powder diffraction (EDXRD) as well as – to some extent – XRF (see Section 2.1.4.3).

An important disadvantage of Si(Li) detectors is their large dead time, which prohibits the handling of higher count rates. Moderate noise levels result in low-to-moderate dynamic ranges. An additional important disadvantage is the limitation to 0D detection.

2.1.7.2.3.2. Silicon micro-strip and silicon pixel detectors

Silicon micro-strip and silicon pixel detectors employ silicon sensors, which are one- or two-dimensional arrays of p–n diodes in the form of strips or pixels, respectively, individually connected to an array of readout channels. The development of this type of detector technology has obviously been driven by the idea of massive parallelism: each strip or pixel actually represents an individual detector. Accordingly, the silicon micro-strip and silicon pixel detectors are therefore of the 1D and 2D detection type, respectively.

Count rates recorded by silicon micro-strip and silicon pixel detectors are very high with very low noise levels, resulting in very large dynamic ranges. The energy resolution of most silicon micro-strip and silicon pixel detectors is of the order of 1600 eV (20%) at 8 keV (Cu radiation). Recently, a silicon micro-strip detector with an energy resolution of better than 380 eV at 8 keV has been introduced (Wiacek *et al.*, 2015). At such high energy resolution Cu Kβ is filtered out to below the detection limit while Mn, Fe and Co fluorescence is filtered completely, allowing this detector to be operated without a metal filter or a diffracted-beam monochromator for most applications.

2.1.7.2.3.3. CCD and CMOS detectors

Charge-coupled device (CCD) detectors are represented by one- or two-dimensional arrays of square or rectangular pixels consisting of metal–oxide–semiconductor (MOS) capacitors, and can detect X-ray photons directly or indirectly. The pixel size may be less than 10 µm. The majority of detectors use indirect detection, where the incoming X-ray photons are first converted to visible-light photons by a phosphor layer. CCD detectors employ the 'bucket brigade' readout method, in which charge is shifted one pixel at a time by phasing the bias on the gate electrodes that overlay each pixel until it reaches the output, resulting in relatively large readout times ranging from a few tenths of a second up to several seconds per frame. Cooling (Peltier-type) is required to reduce the dark-current noise representing the dominant noise source for long exposures. In some detector designs fibre-optic demagnification is used to increase the effective active detector area, resulting in an imaging area larger than the active area of the CCD chip at the cost of detector sensitivity and spatial resolution.

CCD detectors are usually operated as integrating detectors. As such, they have no dead time and therefore provide excellent linearity over a moderate dynamic range, but cannot have energy resolution. CCD detectors are the detectors of choice for single-crystal diffraction and imaging, but are not favourable for applications with weak diffraction signals, such as powder X-ray diffraction, owing to the relatively large dark-current noise.

CCD detectors may also function as counting detectors by making the exposure time sufficiently short. In single-event mode the energy of each photon can be determined, providing an energy resolution down to about 300 eV at 8 keV (Cu radiation) and allowing a spectrum at each pixel of the CCD array to be built up by a series of consecutive measurements. Such a detector can record energy-dispersive X-ray powder diffraction (EDXRD) as well as – to some extent – XRF (see Section 2.1.4.3); however, owing to the readout time, count rates are extremely low with high statistical noise.

Unlike the bucket-brigade readout of a CCD, the complementary metal–oxide–semiconductor (CMOS) active-pixel sensor (He *et al.*, 2011) uses a completely different architecture in which each pixel incorporates a readout preamplifier and is then read out through a bus, as in random-access memory (He *et al.*, 2011). Cooling is not required. CMOS detectors are immune to the blooming effect (in which a light source overloads the sensitivity of the sensor, causing the signal to bleed vertically into surrounding pixels forming vertical streaks). Additionally, they offer the very significant advantage of shutter-free operation, that is dead-time-free continuous scans which improve the efficiency of data collection and also improve data quality by eliminating shutter-timing jitter.

As a consequence of these characteristics, CMOS-detector active-pixel sensors are now replacing CCD chips in a number of high-end applications (*e.g.* professional digital photography and high-definition television), and have reached a level of performance where they are also starting to displace CCD chips in the most demanding scientific applications.

2.1.7.3. *Position sensitivity and associated scanning modes*

2.1.7.3.1. *Pixel size, spatial resolution and angular resolution*

Detectors of the line (1D) or area (2D) type have the important property of position sensitivity, which is characterized by the two parameters pixel size and spatial resolution.

The pixel size of a position-sensitive detector (PSD) can be represented either by the intrinsic size of the smallest addressable sensitive component of a detector (*e.g.* the actual size of the diodes), which can be binned to form larger pixels, or is set by the readout electronics (*e.g.* for wire-based detectors such as proportional counters). The spatial resolution is determined by the actual pixel size, the point-spread function (PSF) and parallax. The PSF represents the spread of a signal produced by a single photon over several pixels by mapping the probability density that a photon is recorded by a pixel in the vicinity of the point that the photon hit. Parallax will lead to an additional smearing if the photon travels at an angle to the detector normal. The final angular resolution of a detector system is given by the spatial detector resolution and the specimen-to-detector distance.

Point (0D) detectors do not provide position sensitivity, regardless of the actual size of the active window (representing a single pixel). Simply speaking, in analogy to PSDs, the spatial resolution of a point detector is determined by the goniometer step size representing the actual pixel size, and the size of the detector slit representing the PSF. As for PSDs, the angular resolution is given by the spatial resolution and the specimen-to-detector distance.

Detectors can be operated in fixed as well as in (2θ) scanning mode, where the step size is usually determined by the detector pixel size. Subsampling, that is scanning using an angular step size smaller than the angular pixel resolution, may be used to improve observed line profile shapes if the pixel resolution is too small. As a rule of thumb some 5–8 data points need be collected over the FWHM of a diffraction peak to allow for an appropriate description of the line-profile shape.

2.1.7.3.2. *Dimensionality*

Area detectors can be operated as line or point detectors. Electronic binning of the pixels into columns will form a line detector, while binning all pixels together will form a point detector, each associated with improvements of count rates and thus dynamic ranges. Alternatively, 1D or 0D 'regions of interest' can be defined electronically and/or by mounting suitable diffracted-beam-path X-ray optics. Area detectors – when operated as such – require point-focus operation.

Line detectors can be used as point detectors, which may be formed in several ways. One way is to only use one or more central pixels by either electronically switching off outer pixels and/or by mounting suitable X-ray optics. Another way is to turn the detector by 90° and to bin all pixels, leading to an improved count rate and thus dynamic range.

Obviously, when turning a line detector by 90°, it will function as an area detector if it is scanned over an angular range; the trace of the scan will form a cylindrical surface that is a two-dimensional diffraction image (He, 2009). This scan mode may be associated with a few advantages, in addition to lower costs. For example, the elimination of parallax and the possibility of using diffracted-beam-path optics improve the angular resolution in the 2θ direction and allow air scattering to be reduced.

2.1.7.3.3. *Size and shape*

PSDs are available in different sizes with flat (1D, 2D), curved (1D), cylindrical (2D) and spherical (2D) detection surfaces. Curved, cylindrical and spherical detectors are designed for focusing or parallel-beam geometries with a fixed specimen-to-detector distance, and cannot normally be used with the Bragg–Brentano geometry because of its 2θ-dependent focusing circle (Section 2.1.4.1). Flat detectors can be used at different specimen-to-detector distances, with either high angular resolution at a large distance or large angular coverage at a short distance. For large flat detectors, parallax errors must be addressed. Small flat detectors are perfectly suited for operation in Bragg–Brentano geometry but the angular coverage should not exceed about 10° 2θ (Section 2.1.4.1) to minimize defocusing, particularly at small 2θ angles.

References

Bartels, W. J. (1983). *Characterization of thin layers on perfect crystals with a multipurpose high resolution X-ray diffractometer*. *J. Vac. Sci. Technol. B*, **1**, 338–345.

Bilderback, D. H. (2003). *Review of capillary X-ray optics from the 2nd International Capillary Optics Meeting*. *X-ray Spectrom.* **32**, 195–207.

Bohlin, H. (1920). *Eine neue Anordnung für röntgenkristallographische Untersuchungen von Kristallpulver*. *Ann. Phys.* **366**, 421–439.

Bonse, U. & Hart, M. (1965). *Tailless X-ray single crystal reflection curves obtained by multiple reflection*. *Appl. Phys. Lett.* **7**, 238–240.

Bowen, D. K. & Tanner, B. K. (1998). *High Resolution X-ray Diffractometry and Topography*. London: Taylor & Francis.

Brentano, J. C. M. (1924). *Focussing method of crystal powder analysis by X-rays*. *Proc. Phys. Soc.* **37**, 184–193.

Charpak, G., Bouclier, R., Bressani, T., Favier, J. & Zupančič, Č. (1968). *The use of multiwire proportional counters to select and localize charged particles*. *Nucl. Instrum. Methods*, **62**, 262–268.

Clearfield, A., Reibenspiess, J. & Bhuvanesh, N. (2008). *Principles and Applications of Powder Diffraction*. New York: Wiley.

Debye, P. & Scherrer, P. (1916). *Interference of X-rays, employing amorphous substances*. *Phys. Z.* **17**, 277–283.

Durst, R. D., Diawara, Y., Khazins, D. M., Medved, S., Becker, B. L. & Thorson, T. A. (2003). *Novel, photon counting X-ray detectors*. *Powder Diffr.* **18**, 103–105.

EN 1330–11 (2007). *Non-Destructive Testing*. Part 11. *Terms used in X-ray Diffraction from Polycrystalline and Amorphous Materials*. Brussels: European Committee for Standardization (CEN).

Fankuchen, I. (1937). *A condensing monochromator for X-rays*. *Nature (London)*, **139**, 193–194.

Fewster, P. F. (2003). *X-ray Scattering from Semiconductors*. London: Imperial College Press.

Friedmann, H. (1945). *Geiger counter spectrometer for industrial research*. *Electronics*, **18**, 132–137.

Göbel, H. E. (1980). *The use and accuracy of continuously scanning position-sensitive detector data in X-ray powder diffraction*. *Adv. X-ray Anal.* **24**, 123–138.

Guinier, A. (1937). *Arrangement for obtaining intense diffraction diagrams of crystalline powders with monochromatic radiation*. *C. R. Acad. Sci. Paris*, **204**, 1115–1116.

Hanawalt, J. D., Rinn, H. W. & Frevel, L. K. (1938). *Chemical analysis by X-ray diffraction*. *Ind. Eng. Chem. Anal.* **10**, 457–512.

Hart, M. (1971). *Bragg-reflection X-ray optics*. *Rep. Prog. Phys.* **34**, 435–490.

He, B. B. (2009). *Two-Dimensional X-ray Diffraction*. New York: Wiley.

He, T., Durst, R. D., Becker, B. L., Kaercher, J. & Wachter, G. (2011). *A large area X-ray imager with online linearization and noise suppression*. *Proc. SPIE*, **8142**, 81421Q.

Hemberg, O. E., Otendal, M. & Hertz, H. M. (2003). *Liquid-metal-jet anode electron-impact X-ray source*. *Appl. Phys. Lett.* **83**, 1483–1485.

Hull, A. W. (1917). *A new method of X-ray crystal analysis*. *Phys. Rev.* **10**, 661–696.

Hull, A. W. (1919). *A new method of chemical analysis*. *J. Am. Chem. Soc.* **41**, 1168–1175.

International Tables for Crystallography (2004). Volume C, 3rd ed., edited by E. Prince. Dordrecht: Kluwer Academic Publishers.

Jenkins, R. & Snyder, B. (1996). *Introduction to X-ray Powder Diffractometry*. New York: Wiley.
Johann, H. H. (1931). *Die Erzeugung lichtstarker Röntgenspektren mit Hilfe von Konkavkristallen*. *Z. Phys.* **69**, 185–206.
Johannson, T. (1933). *Über ein neuartiges, genau fokussierendes Röntgenspektrometer*. *Z. Phys.* **82**, 507–528.
Khazins, D. M., Becker, B. L., Diawara, Y., Durst, R. D., He, B. B., Medved, S. A., Sedov, V. & Thorson, T. A. (2004). *A parallel-plate resistive-anode gaseous detector for X-ray imaging*. *IEEE Trans. Nucl. Sci.* **51**, 943–947.
Kirkpatrick, P. & Baez, A. V. (1948). *Formation of optical images by X-rays*. *J. Opt. Soc. Am.* **38**, 766–774.
Klug, H. P. & Alexander, L. E. (1974). *X-ray Diffraction Procedures for Polycrystalline and Amorphous Materials*, 2nd ed. New York: Wiley.
Kumakhov, M. A. & Komarov, F. F. (1990). *Multiple reflection from surface X-ray optics*. *Phys. Rep.* **191**, 289–350.
Le Galley, D. P. (1935). *A type of Geiger–Müller counter suitable for the measurement of diffracted X-rays*. *Rev. Sci. Instrum.* **6**, 279–283.
Lindemann, R. & Trost, A. (1940). *Das Interferenz-Zählrohr als Hilfsmittel der Feinstrukturforschung mit Röntgenstrahlen*. *Z. Phys.* **115**, 456–468.
Montel, M. (1957). *X-ray microscopy with catamegonic roof-shaped objective*. In *X-ray Microscopy and Microradiography*, pp. 177–185. New York: Academic Press.
Paganin, D. M. (2006). *Coherent X-ray Optics*. Oxford University Press.
Parrish, W. (1949). *X-ray powder diffraction analysis: film and Geiger counter techniques*. *Science*, **110**, 368–371.
Pecharsky, V. K. & Zavalij, P. Y. (2009). *Fundamentals of Powder Diffraction and Structural Characterisation of Materials*, 2nd ed. New York: Springer.
Peiser, M. A., Rooksby, H. P. & Wilson, A. J. C. (1955). *X-ray Diffraction by Polycrystalline Materials*. London: Institute of Physics.
Sauli, F. (1977). *Principle of operation of multi-wire proportional and drift chambers*. CERN 77–09, May 1977.
Schuster, M. & Göbel, H. (1995). *Parallel-beam coupling into channel-cut monochromators using curved graded multilayers*. *J. Phys. D Appl. Phys.* **28**, A270–A275.
Schuster, M. & Göbel, H. (1996). *Application of graded multilayer optics in X-ray diffraction*. *Adv. X-ray Anal.* **39**, 57–72.
Seemann, H. (1919). *Eine fokussierende röntgenspektroskopische Anordnung für Kristallpulver*. *Ann. Phys.* **364**, 455–464.
VDI/VDE Guideline 5575 Part 3 (2011). *X-ray Optical Systems: Capillary X-ray Lenses*. Berlin: Beuth.
VDI/VDE Guideline 5575 Part 4 (2011). *X-ray Optical Systems: X-ray Mirrors. Total Reflection Mirrors and Multilayer Mirrors*. Berlin: Beuth.
Wiacek, P., Dabrowski, W., Fink, J., Fiutowski, T., Krane, H.-G., Loyer, F., Schwamberger, A., Świentek, K. & Venanzi, C. (2015). *Position sensitive and energy dispersive X-ray detector based on silicon strip detector technology*. *J. Instrumen.* **10**, P04002.